ELSEVIER

S0309-1708(96)00037-1

Advances in Water Resources **21**, No. 2, pp. 121–143, 1998

0309-1708/98/$17.00+0.00

Three-dimensional modeling of three phase imbibition and drainage

Darryl H. Fenwick & Martin J. Blunt

Department of Petroleum Engineering, Stanford University, CA 94305-2220, USA

(Received 15 September 1995; accepted 12 July 1996)

This paper investigates three phase flow in water-wet porous media. From considerations of capillary equilibrium and an analysis of micromodel experiments, the pore scale displacement mechanisms are described. The stability of layers of NAPL between water and gas has an important impact upon the recovery of NAPL to low saturation. The displacement mechanisms and the effects of NAPL layers are incorporated into a three-dimensional network model. The network model calculates capillary pressure, relative permeability, and NAPL recovery. Several types of displacement are analyzed by specifying a series of changes in capillary pressure. Different capillary pressure paths result in drastically different relative permeabilities and NAPL recoveries. In ideal circumstances, the ultimate recovery of NAPL can be virtually 100%, but the recovery time is governed by flow through NAPL layers, which is shown to be very strongly influenced by the boundary condition at the fluid interfaces. The relative permeabilities and capillary pressures we calculate cannot be adequately represented by current empirical models. Copyright © 1996 Elsevier Science Limited

Key words: network modeling, three phase flow, relative permeability, capillary pressure, pore scale, multiphase flow in porous media.

1 INTRODUCTION

Three phase flow in porous media occurs in oil and gas reservoirs as well as during groundwater contamination and cleanup. Most improved oil recovery projects involve the flow of three phases, where a gas phase, which could be air, natural gas, CO_2, N_2, or steam, is injected into a reservoir containing water and oil. Gas injection works because oil will flow at a lower saturation in the presence of gas and water than with water alone. The flow of a nonaqueous phase liquid (NAPL) through the vadose zone toward the water table, which occurs when a surface storage tank leaks, is also a three phase flow process. In environmental contexts, NAPL may be flowing at saturations of 1% and lower — again the presence of both water and air may allow the NAPL to be displaced to lower saturation than in either completely dry soil or fully saturated soil.

The modeling of multiphase flow in porous media requires knowledge of the capillary pressure and relative permeability functions.[1] Capillary pressure is defined as,

$$P_{cij} = P_i - P_j \tag{1}$$

where the subscripts label the three phases, gas (air), NAPL, and water. P_i is the pressure of phase i. Relative permeabilities (k_{ri}) are defined by the multiphase Darcy law,

$$v_i = -\frac{Kk_{ri}}{\mu_i}\nabla(P_i - \rho_i g z), \tag{2}$$

where v_i is the Darcy velocity of phase i, μ is the viscosity, ρ is the density, g is the gravitational acceleration, K is the absolute permeability, and z is the vertical coordinate.

Most numerical models of three phase flow rely on empirical relationships between capillary pressure, saturation, and relative permeability.[15,41,48,49,50] It is very difficult to measure relative permeability and capillary pressure for the full range of possible three phase saturations and saturation histories (see Oak *et al.*[36] for a listing of relative permeability studies up to 1990). Baker,[3] Delshad and Pope,[9] and Oak[35] compared empirical models to published experimental data. With only a few exceptions they showed that empirical models could not match the measured relative permeabilities.

Empirical models fail because they do not account for the physics of flow. All three phase models assume that the capillary pressure and relative permeabilities are

unique functions of saturation and independent of fluid properties. As we will show later, this is not the case and such assumptions make large errors, particularly for flow at low NAPL saturations, which is the case of greatest practical interest.

One way of incorporating physics into the prediction of relative permeability is through pore level modeling. To simulate the flow accurately, a proper understanding of the pore scale displacement mechanisms is necessary. Due to the tremendous geometrical complexity of the pore space as well as the fluid–fluid interactions, this is a very difficult task which has not been fully accomplished. However, a great deal of experimental work studying two phase flow at the pore scale has been performed, especially for strongly water-wet systems. From extensive experimental studies in micromodels (see for instance the work of Lenormand and Zarcone[27]), the pore level mechanisms for two phase flow are well understood. When these mechanisms are coded into a numerical model, the two phase flow behavior for both consolidated and unconsolidated media, including capillary pressures and relative permeabilities can be predicted successfully.[5,7,19,21,28]

Pore level processes in three phase flow are less well understood. However, some three phase network models have already been presented. Among the first was a model by Heiba *et al.*[18] that used percolation theory to calculate three phase relative permeabilities. However, percolation theory doesn't account for many of the important features of three phase flow, which we will describe later, and the relative permeabilities were calculated for a simplified lattice that does not resemble realistic porous media. Soll and Celia[46] presented a three phase model that contained physical insight into three phase flow obtained from micromodel experiments by Soll *et al.*[47] Soll and Celia[46] were able to match the capillary pressure curves of the micromodel experiments as well as some laboratory column tests. The authors did not calculate relative permeabilities. Øren and Pinczewski[39] created a network model that also contained the pore scale displacement mechanisms that were observed in previous micromodel experiments.[37,38] They predicted the residual NAPL saturations after gas injection as well as the patterns of gas invasion into the micromodel. However, Øren and Pinczewski[39] did not calculate relative permeability functions either, and their results were only for two-dimensional systems.

This paper presents a three-dimensional pore level network model that includes the pore level displacement mechanisms found by Øren *et al.*[38] and Soll *et al.*[17] In addition, we identify several other displacements that have not been previously mentioned. A unique feature of three phase flow is the ability of NAPL to form a stable layer between water and gas in the pore space. It is the stability and conductance of this layer which is the principal determinant of NAPL flow at low saturation. Our model includes a consistent treatment of NAPL layer flow which resolves previously conflicting interpretations of three phase flow experiments. This subject is treated in the next section. The pore level displacement processes in two and three phase flow are analyzed next, and then our network model is described.

2 NAPL FILMS AND LAYERS

It has long been known that many NAPLs can spread between gas and water.[2] The spreading of a NAPL on water in the presence of air is determined by the equation that defines the initial spreading coefficient,

$$C_s^I = \gamma_{gw} - (\gamma_{nw} + \gamma_{gn}), \tag{3}$$

where γ is the interfacial tension, the subscript g indicates a gas, w indicates water, and n denotes NAPL. Note that the interfacial tensions are for pure fluids initially in contact with each other. Figure 1a shows that eqn. (3) represents a force balance at the three phase contact line of water/NAPL/gas. If $C_s^I > 0$, there is no configuration of the fluids that balances the forces in the horizontal direction. Thus, the NAPL spreads over the surface of the water.

When the NAPL is present on the gas/water interface, either through spreading or through adsorption from the vapor phase, γ_{gw} is reduced and can be defined as an effective gas/water interfacial tension, γ_{gw}^e. The other interfacial tensions are also modified in the presence of a third phase (denoted γ_{nw}^e and γ_{gn}^e), but it is the value of γ_{gw}^e that is most dramatically affected.[2] When the three phases are at thermodynamic equilibrium, the equilibrium spreading coefficient can be defined as,

$$C_s^{eq} = \gamma_{gw}^e - (\gamma_{nw}^e + \gamma_{gn}^e). \tag{4}$$

The equilibrium spreading coefficient must be less than or equal to zero.[44] If $C_s^I > 0$ and $C_s^{eq} = 0$, NAPL spreads as a film which will swell as more NAPL is added to the system (Fig. 1b). This is the case for Soltrol.[40] If $C_s^{eq} < 0$ and $C_s^I > 0$, the NAPL will spread initially, but finite contact angles between the phases can exist such that excess NAPL will be found in droplets connected by thin films on the gas/water interface (Fig. 1c). This the case for benzene[2] as well as hexane and heptane.[20] The film of NAPL is generally very thin, on the order of one nanometer across (10^{-9} m).[20]

When gas contacts NAPL in a water-wet porous medium, the three phases behave in the same way as described above for flat films shown in Fig. 1. If the initial spreading coefficient is positive, the NAPL will spread between the gas and water forming a continuous film. The ability of the NAPL to reside between water and gas has important implications for the recovery of NAPL in porous media. Final NAPL saturations as low as 0·1% have resulted from the displacement of NAPL in the presence of both water and gas.[52] Studies by Chatzis *et al.*,[8] Kalaydjian,[24] Kalaydjian *et al.*,[25] and

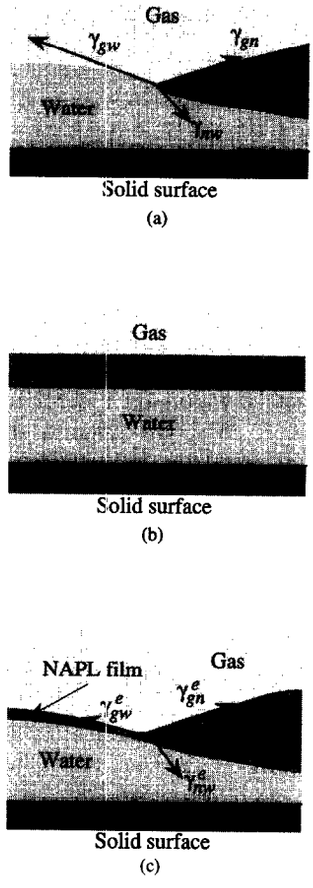

Fig. 1. (a) NAPL initially resting on water in the presence of gas. This arrangement is only stable if $C_s^I < 0$. (b) The configuration of three phases when $C_s^{eq} = 0$. (c) The configuration when $C_s^I > 0$, and $C_s^{eq} < 0$.

Vizika[51] have shown a significant difference in the ultimate recovery of NAPL between systems with positive and negative spreading coefficient. It has been suggested that high recovery is due to the existence of films of NAPL between the water and gas when $C_s^I > 0$, creating a continuous channel of NAPL through which it can drain,[6,8,14,26,51] whereas when $C_s^I < 0$ such films are absent and the NAPL recovery is lower.

However, the simple theory that high NAPL recovery is due to films caused by spreading may not explain several other gravity drainage studies where similar recoveries were observed for both positive and negative C_s^I. Table 1 gives several references reporting residual NAPL saturations after gas injection (S_{nrg}) in water-wet porous media. Note that the experiments in the references given were not identical, so direct comparisons cannot be made. The references indicate a difference in recovery between $C_s^I < 0$ and $C_s^I > 0$. However, the difference is sometimes very slight, and the high NAPL recoveries observed for $C_s^I < 0$ indicate that there may be other factors involved in the recovery of NAPL in the presence of gas than simply the value of C_s^I.

These seemingly contradictory studies can be resolved by realizing that thick NAPL layers between water and gas in crevices of the pore space can be thermodynamically favorable even for systems with a negative spreading coefficient. Dong *et al.*[11] performed free energy calculations and found that a NAPL can reside between water and gas in the corners of the pore space as shown in Fig. 2a for systems with $C_s^I < 0$. Note that the term NAPL layer will be employed to distinguish NAPL residing in corners of the pore space, as shown for an idealized angular wedge in Fig. 2, from the thin molecular-sized NAPL films on a flat surface in Fig. 1. A NAPL layer may be several microns across, thousands of times thicker than a film. The ability of the NAPL to form a layer depends on the equilibrium spreading coefficient, the capillary pressures, and the angle β of the corner.[11] Calculation of NAPL flow rates through films show that they are very small,[6] and thus the excellent NAPL recoveries observed experimentally must be due to drainage of much thicker NAPL layers in crevices in the pore space. Experimental evidence for the existence of films in nonspreading systems was found by Hayden and Voice,[17] who performed experiments on iodobenzene and found layers and films to exist even though $C_s^I = -8{\cdot}7$ mN/m. Evidence to support the idea that the equilibrium spreading coefficient, not initial spreading coefficient, determines NAPL layer stability is the calculations of the speed of spreading films, which is much greater than phase velocities in porous media displacements.[22] Thus, all gas/water interfaces will rapidly become polluted by NAPL, and the spreading coefficient will rapidly approach the value at equilibrium.

Table 1. Reported experimental recoveries for different spreading coefficients using water-wet porous media

Reference	S_{nrg}, $C_s^I > 0$ (%)	S_{nrg}, $C_s^I < 0$ (%)
Dumoré & Schols[14]	2·9%	3·2%
Kantzas *et al.*[26]	0·6–9·1	no values
Vizika[51]	11	23
Kalaydjian *et al.*[25] (Clashach sandstone)	10	31
Kalaydjian *et al.*[25] (Fountainbleu sandstone)	16	20
Skurdal *et al.*[45]	4·7	6·7
Zhou & Blunt[52]	0·13–1·49	0·35–5·25

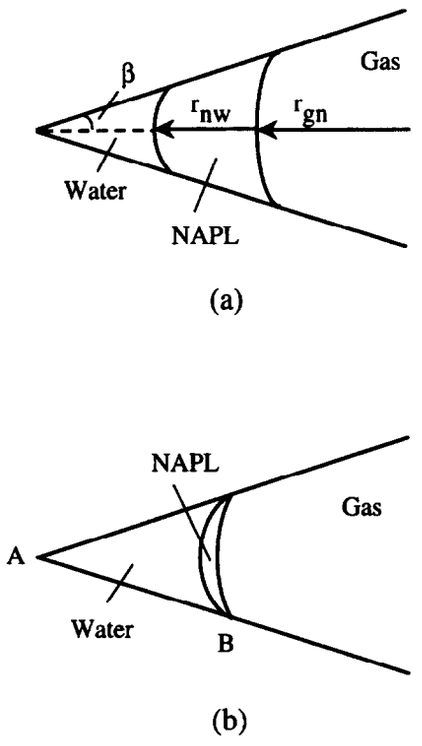

Fig. 2. (a) Three phases in a corner with half angle β. (b) When the gas/NAPL and NAPL/water interfaces touch at point B, we assume that the NAPL layer is first unstable.

Fenwick and Blunt[16] developed a simple model to capture the proposed NAPL layer behavior. Figure 2 depicts three phases in a wedge found in the pore space. The fluids are assumed to behave as depicted, that is, that the solid is water-wet, the NAPL/water contact angle (θ_{nw}) is smaller than the gas/NAPL contact angle (θ_{gn}), and that the only curvature of the interface is in the plane of the wedge. Thus, using the Young–Laplace equation, the NAPL/water capillary pressure is given by $P_{cnw} = \gamma_{nw}/r_{nw}$, where r_{nw} is the radius of curvature of the NAPL/water interface, with a similar expression for the gas/NAPL capillary pressure (P_{cgn}). We assume that the NAPL layer is stable until the contact of the NAPL/water interface with the solid surface coincides with the gas/NAPL contact, as shown in Fig. 2b. For an interface of radius r, contact angle of θ, and wedge of half angle β, the distance AB in Fig. 2b is

$$\mathrm{AB} = r\frac{\cos(\theta+\beta)}{\sin\beta}. \tag{5}$$

Note that if $\theta + \beta > \pi/2$, no stable configuration of the wetting fluid can exist in the wedge (the curvature would be negative). For the cases investigated here, $\theta + \beta < \pi/2$. A ratio of interfacial curvatures can be defined as,

$$R = \frac{r_{nw}}{r_{gn}} = \frac{P_{cgn}\gamma_{nw}}{P_{cnw}\gamma_{gn}} \tag{6}$$

If R is very small, then the NAPL layer can be very thick. For $R = 0$, only NAPL is found in the wedge. The critical ratio R_c at which the layer is no longer stable is from eqn. (5),

$$R_c = \frac{\cos(\theta_{gn}+\beta)}{\cos(\theta_{nw}+\beta)} \tag{7}$$

If $R < R_c$, then the fluid arrangement resembles Fig. 2a. If $R > R_c$, we assume that there is no NAPL layer, and there is only a gas/water interface with an interfacial tension γ^e_{gw}. Although there might be a molecular-sized NAPL film present, this film is too thin to have any significant effect on the flow of NAPL.[6]

For a completely water-wet system it is possible to relate θ_{gn} to C_s^{eq}. We will assume throughout this paper that water coats the entire solid surface with a molecular film and the system is strongly water-wet ($\theta_{nw} = \theta_{gw} = 0$). At the gas/NAPL/solid contact, the horizontal force balance of the interfacial tensions is given by,

$$\gamma_{gw} = \gamma_{gn}\cos\theta_{gn} + \gamma_{nw}. \tag{8}$$

Equation (8) can be manipulated, resulting in,

$$\cos\theta_{gn} = 1 + \frac{C_s^{eq}}{\gamma_{gn}}, \tag{9}$$

as described by Kalaydjian[24] and Kalaydjian *et al.*[25] Using eqn. (9), eqn. (7) becomes,

$$R_c = 1 + \frac{C_s^{eq}}{\gamma_{gn}} - \left(-\frac{C_s^{eq}}{\gamma_{gn}}\right)^{1/2}\left(2 + \frac{C_s^{eq}}{\gamma_{gn}}\right)^{1/2}\tan\beta \tag{10}$$

It should be emphasized again that eqn. (10) is based upon a simplified geometric argument for NAPL layer stability. However, the analysis gives an indication of the expected behavior of NAPL layers. Layers can be present even for negative spreading coefficients, but as the spreading coefficient decreases, NAPL layers become increasingly less likely to exist. Notice that whether or not a NAPL layer exists depends on the value of R which is governed by the ratio of capillary pressures, and on R_c which depends on C_s^{eq}. Thus NAPL layers may be present for $C_s^{eq} < 0$, and absent for $C_s^{eq} = 0$, depending on the capillary pressures.

3 DISPLACEMENT MECHANISMS

3.1 Structure of the porous medium

Most micromodel studies have been performed on two-dimensional networks of rectangular channels.[27] We model the a porous medium with a similar structure in three dimensions — i.e. the porous medium may be represented as a network of narrow chambers (called throats) that intersect at larger void spaces (called pores), as illustrated in Fig. 3. Moreover, the pore space is assumed to contain connected roughness, grooves or crevices that act as conduits for the wetting fluid, even if

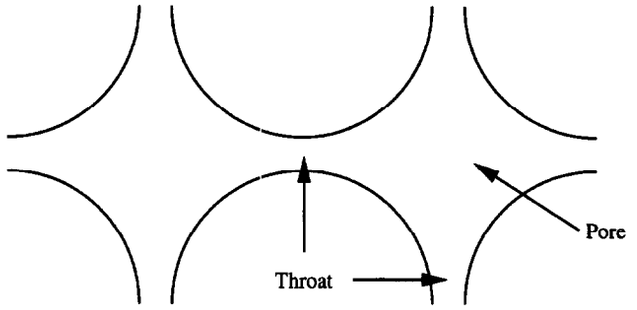

Fig. 3. Schematic diagram of a porous medium with large void spaces, called pores, connected by small chambers, called throats.

the center of the pore or throat is filled with nonwetting fluid, as shown in Fig. 4 for a throat of square cross-section. The implication is that the wetting phase is never trapped and can reach a low saturation given enough time. Experiments by Dullien *et al.*[13] have shown that in strongly water-wet media, wetting phase saturations as low as 1% are possible. Note that if NAPL layers are stable, the NAPL is always connected and can never be trapped. This would appear to be a reasonable approximation, since as mentioned previously, NAPL saturations as low as 0.1% have been achieved (see Table 1).

3.2 Two phase mechanisms

Two phase displacement mechanisms have been described most extensively by Lenormand *et al.*[29] and Lenormand and Zarcone.[27] When a nonwetting fluid displaces a wetting fluid, such as when NAPL or gas invades water, or gas displaces NAPL, the process is called drainage. Drainage is characterized by piston-like displacement, which is depicted in Fig. 5. At every stage in the displacement the nonwetting fluid invades the pore or throat with the lowest threshold capillary pressure.

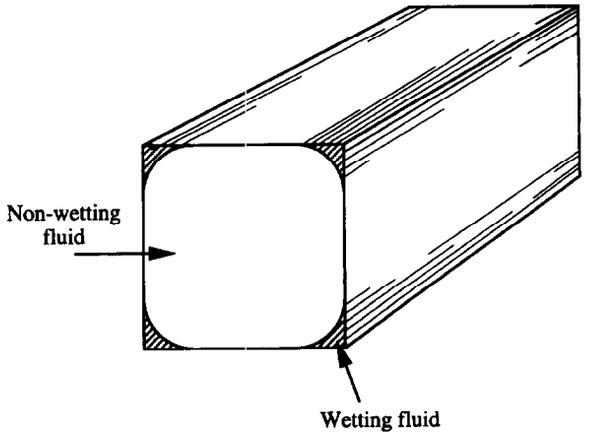

Fig. 4. The wetting fluid can bypass the nonwetting fluid by flowing in the corners and wedges of the pore space, shown here for a throat of square cross-section.

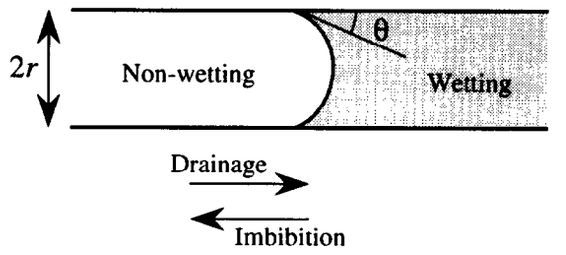

Fig. 5. Piston-like displacement in a pore of radius r with contact angle θ between the phases.

However, the nonwetting fluid may only fill a pore or throat that is adjacent to an already filled region of the pore space. The critical capillary pressure for the invading phase to enter a pore or throat of inscribed radius r with contact angle θ is approximately,

$$P_c = \frac{2\gamma\cos\theta}{r}. \tag{11}$$

If the difference in pressure between the nonwetting and wetting phases is larger than $2\gamma\cos\theta/r$, displacement occurs.

Imbibition occurs when a wetting fluid invades a nonwetting fluid, such as water or NAPL into gas, or water into NAPL. Here the wetting fluid fills a pore or throat with the highest threshold capillary pressure. Since the wetting phase is assumed to be connected through layers in the corners and grooves throughout the pore space (Fig. 4), the wetting fluid is able to displace nonwetting fluid in every pore or throat. The wetting layers can be either water or NAPL layers (if they are present). There are two types of displacement. The first is snap-off,[43] illustrated schematically in Fig. 6. As imbibition proceeds and the capillary pressure decreases the radius of curvature of the fluid interface in a throat increases until a point of instability is reached when the interface no longer touches the solid, and the throat spontaneously fills with wetting fluid. For a throat of square cross-section and inscribed radius r, the critical capillary pressure at which this occurs is,[27]

$$P_c = \frac{\gamma(\cos\theta - \sin\theta)}{r}. \tag{12}$$

The second type of displacement is piston-like invasion shown in Fig. 5. For a given throat piston-like invasion has a higher capillary pressure (eqn. (11)) than snap-off, and so is favored, but can only occur if the adjacent pore or throat is already completely filled with wetting phase. The critical pressure for piston-like pore filling depends on the number of adjacent throats that are completely filled with wetting fluid. This is discussed in detail by Lenormand and Zarcone.[27] They described the piston-like displacements as I_n, where n pore throats are filled with nonwetting fluid. The displacement is most favored for small n. An example of an I_1 mechanism is shown in Fig. 7. The capillary pressure for the I_1

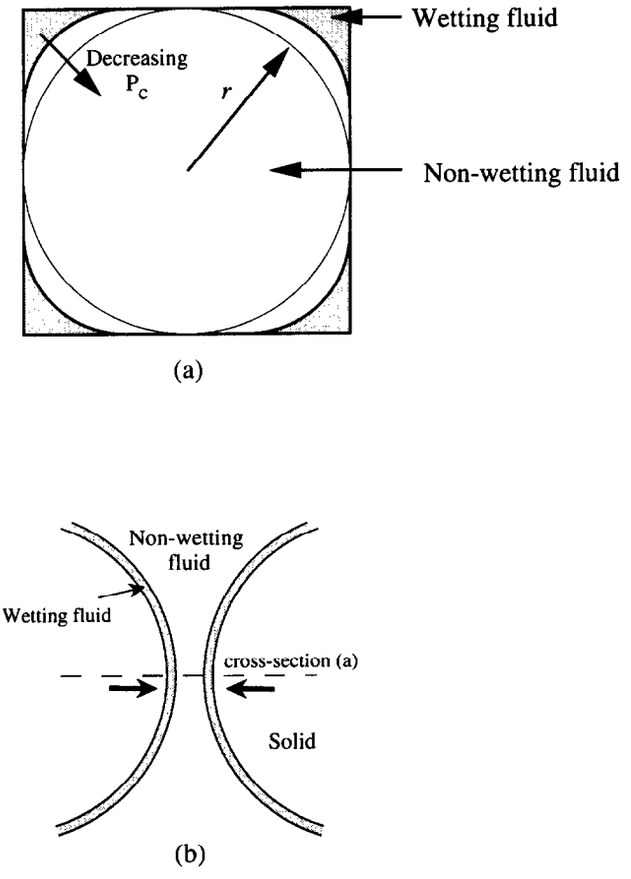

Fig. 6. A schematic of snap-off in a throat with a square cross-section. (a) The cross-section of the throat, where r is the maximum inscribed radius of the square. During imbibition, the capillary pressure decreases, increasing the interfacial radius of curvature. The wetting fluid swells in the corners of the throat until the entire throat fills with the wetting fluid. Snap-off occurs in the smallest constriction in the throat, denoted by the arrows in (b).

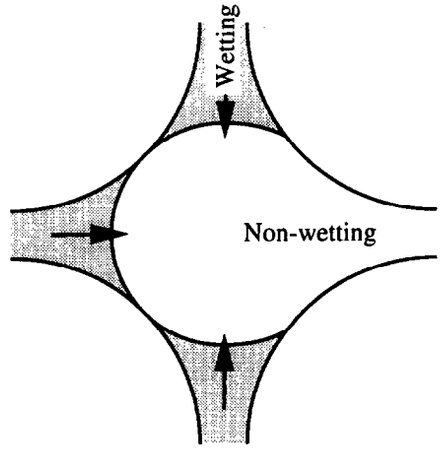

Fig. 7. I_1 displacement of NAPL by water in a pore with four connecting pore throats.

displacement for a pore of inscribed radius r is approximately,

$$P_c = \frac{C_{I_1}\gamma}{r}, \tag{13}$$

where C_{I_1} is a constant slightly less than 2, depending on the pore geometry, the contact angle, and the number of adjacent throats next to the pore. For the I_2 displacement, the constant C_{I_2} will be smaller than C_{I_1}. Since pores are always larger than their adjacent throats, piston-like advance in pores is always favored over snap-off. The nonwetting phase may be trapped if it is completely surrounded by wetting fluid. In this case no further displacement is possible in a capillary controlled displacement.

3.3 Three phase mechanisms

When three phases are present in the pore space, a new series of displacements is possible. We call this double displacement, because one fluid displaces another which displaces the third. For a double displacement to be possible, the first and third phase must be continuous in the pore space. For instance, if the water table containing trapped NAPL is lowered, gas is introduced into the pore space, enabling gas to invade water (two phase displacement), or gas to invade NAPL which then displaces water (double displacement). Øren *et al.*[38] observed several gas → NAPL → water displacements in a micromodel (the → can be replaced by the word 'displaces'), and called this displacement sequence double drainage. Double drainage can mobilize residual (trapped) NAPL and contributes to the reduction of residual NAPL saturation in the presence of gas and water. Figure 8 depicts a double drainage event. The gas and water must be continuous for double drainage to occur. We assume the water is strongly wetting and always continuous. The critical gas/water capillary pressure P_{cgw} for the double drainage displacement is the summation of the capillary pressures of the individual two phase displacements. Thus, for Fig. 8, the critical capillary pressure is,

$$P_{cgw} = 2\gamma_{gn}\cos\theta_{gn}/r_{tgn} + 2\gamma_{nw}/r_{tnw}, \tag{14}$$

where r_{tgn} and r_{tnw} are the critical radii of curvature in the throats as shown in Fig. 8. Note again that in this work we assume that $\theta_{nw} = \theta_{gw} = 0$. If P_{cgw} is above this value, then double drainage can occur.

The converse of double drainage is double imbibition (water → NAPL → gas), illustrated in Fig. 9. Note again that for double imbibition to be possible, the gas must be continuous. The critical capillary pressure required for the displacement in Fig. 9 to occur is given by $P_{cgw} = P_{cnw} + P_{gn}$, or,

$$P_{cgw} = \gamma_{nw}/r_{tn} + 2\gamma_{gn}\cos\theta_{gn}/r_{tg}, \tag{15}$$

where the first term is for snap-off in a throat (eqn. (12)

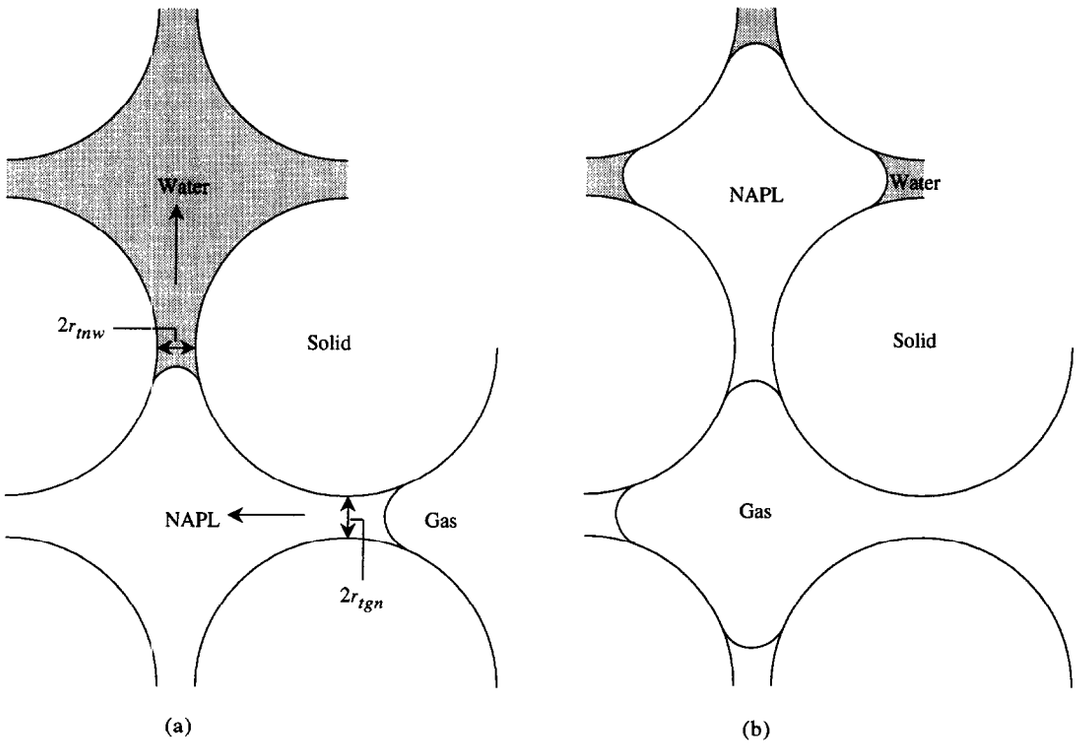

Fig. 8. A schematic double drainage displacement. (a) NAPL contacts gas and water-filled pores or throats. (b) Gas invades into NAPL, which in turn displaces water.

with $\theta = 0$) and the second term is for piston-like advance (eqn. (11)). Since this is an imbibition process, P_{cgw} must be below the critical value for the displacement to occur.

By considering all possible double displacements, it is easy to show that six double displacements are possible, and they are summarized in Table 2. The critical capillary pressure for any double displacement to occur is found by summing the two phase capillary pressures.

4 NETWORK MODELING

The network model presented is a conceptual representation of a porous medium. Pore throats connect larger pore bodies to form a network that contains an inlet and an outlet face. The network model presented here has a cubic lattice with a coordination number of six, which means that six pore throats are connected to each pore. Most porous media have average coordination numbers

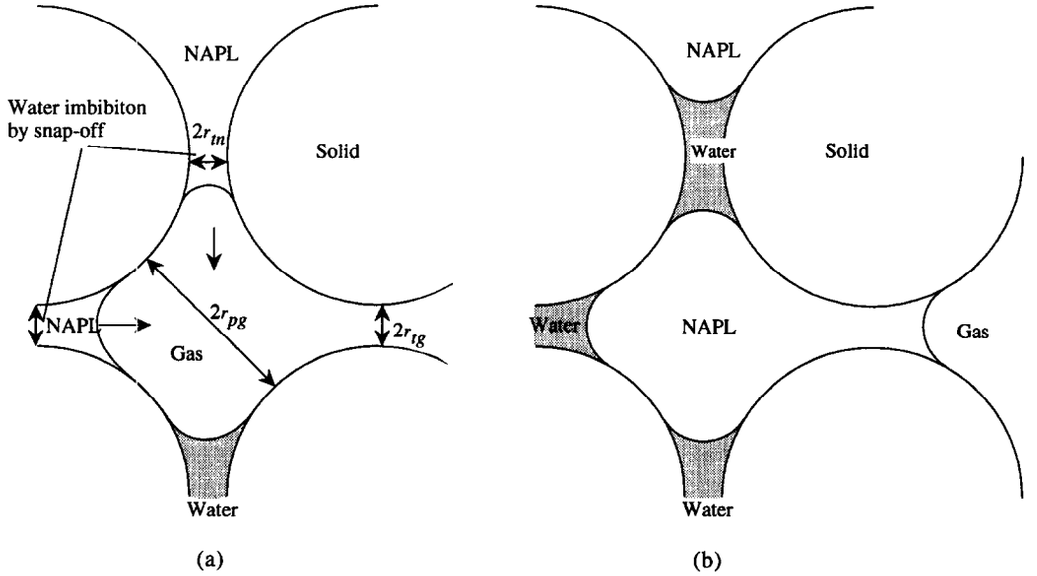

Fig. 9. A schematic double imbibition displacement. (a) Water invades into NAPL that contacts gas. (b) NAPL subsequently displaces the gas.

Table 2. Summary of double displacement mechanisms in three phase flow

Mechanism	Name
Drainage	
Gas → NAPL → water	Double drainage, DD
Gas → water → NAPL	Drainage–imbibition, DDI
NAPL → gas → water	Imbibition–drainage, DID
Imbibition	
NAPL → water → gas	Drainage-Imbitition, IDI
Water → gas → NAPL	Imbibition–drainage, IID
Water → NAPL → gas	Double imbibition, II

between four and eight.[21] Jerauld and Salter[21] performed two phase network model simulations on a cubic lattice and were able to obtain the generic hysteresis behavior for two phase flow. Jerauld and Salter[21] also found that the relative permeabilities for regular and random lattices with the same coordination number are 'nearly identical'.[21] We therefore assume that a regular cubic lattice will generate hysteresis in three phase flow representative of soil and rock. However, different coordination numbers will affect the capillary pressure and relative permeability curves.[21,31,34] Nilsen *et al.*[34] calculated two phase relative permeabilities with various coordination numbers, and found that the wetting phase relative permeabilities were not significantly affected. We would expect similar results for three phase relative permeabilities.

Periodic boundary conditions are used in the directions perpendicular to the inlet/outlet direction. The periodic boundary conditions help to minimize finite size effects in the results. For the model presented here, the pores and throats have a constant square cross-section with sides twice the length of the largest inscribed radius. The pores are assumed to be cubes. Square cross-sectional pores and throats are, of course, a simplification from the complex geometry of real porous media. However, they do allow the wetting fluid to reside in the corners.

The pore and throat size distributions for the inscribed radius used in this paper are shown in Fig. 10. These were determined by using a formula taken from a truncated Weibull distribution.[10] To obtain the largest inscribed radius for a throat, a random number $x \in [0, 1]$ is drawn, and a value y distributed between 0 and 1 is obtained by,

$$y = (-\beta \ln[x(1 - e^{-1/\beta}) + e^{-1/\beta})])^{1/\alpha}, \tag{16}$$

where $\alpha > 0$. The radius is found by scaling y between the minimum ($r_{t\min}$) and maximum radius ($r_{t\max}$) for a throat,

$$r_t = (r_{t\max} - r_{t\min})\, y + r_{t\min}. \tag{17}$$

Equations (16) and (17) were also used to find the lengths of the throat and aspect ratios for the pores. Table 3 gives the cutoff minimum and maximum values as well as α and β used for each distribution for the simulations presented. The inscribed radius for each pore is found by multiplying the aspect ratio by the average size of the six connecting throat radii. If that value is smaller than the largest connecting throat, the pore is set to the size of that throat.

The distributions in Fig. 10 were not selected from a distribution from an actual porous medium, but are consistent with distributions used in other work.[21] Although results from only one set of distributions is presented, capillary pressures and relative permeabilities for various distributions have been calculated. The results are qualitatively similar for all distributions investigated.

4.1 How the network model simulates fluid invasion

The network model performs displacements based upon maintaining capillary equilibrium between the phases. Displacements are performed one pore or throat at a time. Each available pore or throat that can be invaded by a given phase has a critical capillary pressure associated with it that corresponds to a particular type of displacement. When a phase is selected to invade into the network, the pores and throats that are invaded are filled in order of increasing phase pressure. Thus, in drainage, the largest accessible pore or throat corresponding to the smallest capillary pressure is invaded first. In imbibition, the smallest pore or throat corresponding to the largest capillary pressure is invaded first. For example, for gas invasion into water and disconnected NAPL ganglia, the displacement associated with the smallest gas pressure (smallest P_{cgw}) is performed. This could be either a double drainage or gas → water displacement.

Explicit in this rule-based displacement process is the assumption that capillary forces control the displacement at the pore scale. This is not a limiting assumption, since most three phase displacements occur at very small velocities away from wellbores.

4.2 How saturations are calculated

The phases are all assumed to be incompressible. Thus the phase saturations are not a function of the magnitude of phase pressures — they are functions only of the fluid/fluid interfacial curvatures.

The total volume of each throat and pore is given by,

$$V_t = 4r_t^2 L, \qquad V_p = 8r_p^3, \tag{18}$$

where r_t is the inscribed throat radius, r_p the inscribed pore radius, and L is the length of the throat. When two or three phases occupy a pore or throat, the wetting phase (water) resides in the corners of the pore space. The water volume in the corner of a pore is given by,

$$V_{wp} = 8r_{wp}^3 - \tfrac{4}{3}\pi r_{wp}^3, \tag{19}$$

where r_{wp} is the interfacial radius of curvature between the water and the contacting nonwetting fluid given by

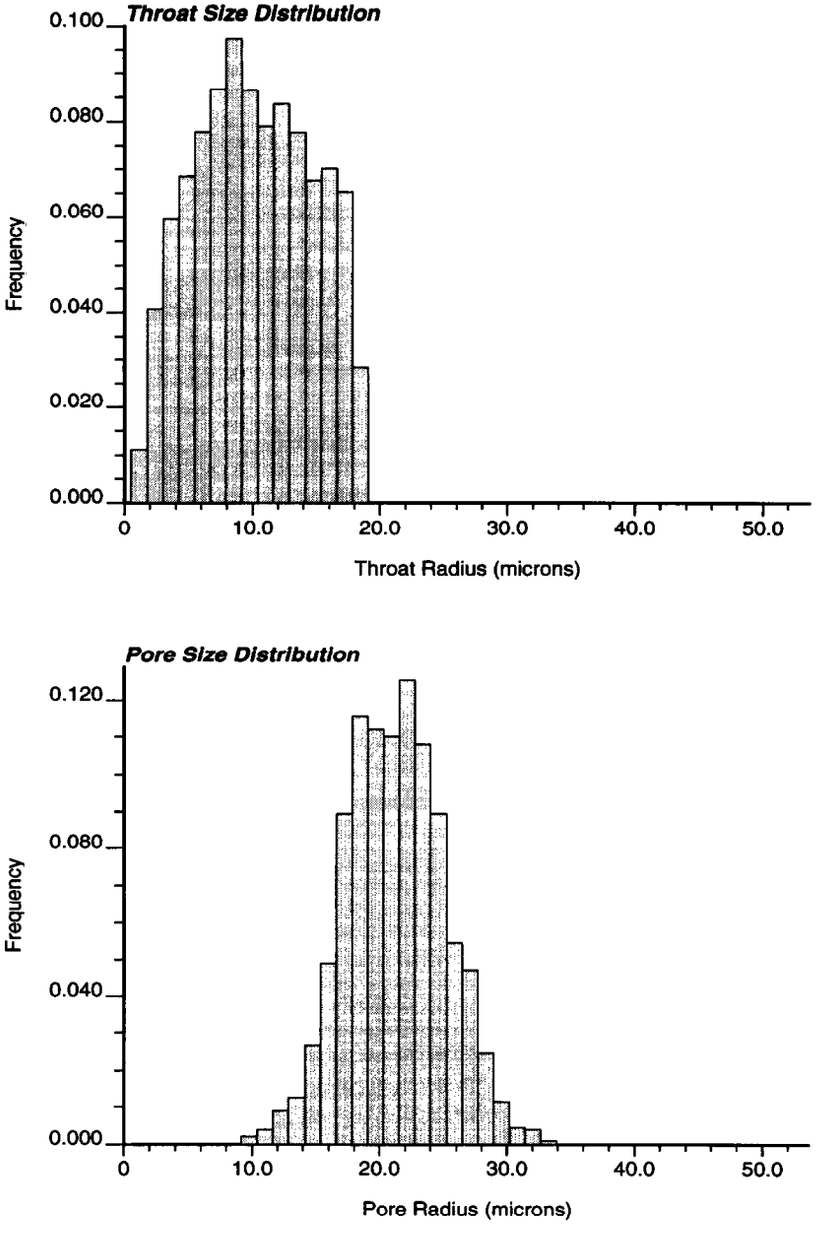

Fig. 10. Throat and pore size distributions for the network model simulations. These distributions are calculated with a truncated Weibull cumulative distribution function.[10]

$r_{wp} = 2\gamma/P_c$. The water volume in the corner of a throat is given by,

$$V_{wt} = (4r_{wt}^2 - \pi r_{wt}^2)L, \tag{20}$$

where L is the length of the throat and $r_{wt} = \gamma/P_c$. Note that we assume that in the throats the interface is curved in only one direction. If two phases reside in the pore or throat, the nonwetting phase volume is taken by subtracting V_{wp} or V_{wt} from V_t or V_p as appropriate.

If three phases reside in the pore or throat with NAPL in a layer, the calculation for the water volume is the same, with $r_{wt} = r_{nw}$ or $r_{wp} = r_{nw}$ and $r_{nw} = \gamma_{nw}/P_{cnw}$. The volume of a NAPL layer in a throat of length L is calculated by,

$$V_n = \left[r_{gn}^2\left(\frac{\cos(\theta_{gn}+\beta)}{\sin\beta}(\cos(\theta_{gn}+\beta)\cos\beta + \sin(\theta_{gn}+\beta)\sin\beta) - \frac{\pi}{2} + \theta_{gn} + \beta\right) - r_{nw}^2\left(\cot\beta - \frac{\pi}{2} + \beta\right)\right]L, \tag{21}$$

Table 3. Parameters used to calculate pore and throat size dimensions

	Minimum	Maximum	α	β
Aspect ratio	2	2·2	1	1·2
Throat radius (μm)	1	18·5	1·6	0·8
Throat length (μm)	40	55	1·6	0·8

where $r_{gn} = \gamma_{gn}/P_{cgn}$ and $r_{nw} = \gamma_{nw}/P_{cnw}$ and β is the half angle of the throat ($\pi/4$ for square cross-section). For a pore, replace L by $2r_p$ in eqn. (21). The gas volume is calculated by subtracting the water and NAPL volumes from the total volume of the pore.

As the capillary pressure changes, the radius of curvature between the continuous phases changes. If the nonwetting phase (NAPL or gas) in the pore or throat is trapped, the radius of curvature is constant and is determined by the capillary pressure between the phases when the nonwetting phase was trapped. To calculate the saturation in the network model, the phase volumes in each pore and throat are found using eqns. (18)–(21). The total pore volume of the network is determined during initialization. Thus, given the volumes of each phase at the current capillary pressures, the saturation is determined by dividing the volume of each phase by the total pore volume of the network.

4.3 How relative permeability is calculated

Note again that the phases are assumed to be incompressible, so for each pore i the equation,

$$\sum_{j}^{Z} q_{ij}^{\alpha} = 0, \tag{22}$$

is obeyed, where q_{ij}^{α} is the volumetric flow rate of phase α between pore i and neighboring pores j. The value Z is the coordination number of pore i. The flow rate q_{ij}^{α} is defined as,

$$q_{ij}^{\alpha} = g_{ij}^{\alpha}(P_i^{\alpha} - P_j^{\alpha}), \tag{23}$$

where g_{ij}^{α} is the conductance of phase α between the pores i and j. The conductance g_{ij}^{α} is the harmonic mean of the conductances between the centers of pores i and j,

$$\frac{1}{g_{ij}^{\alpha}} = \frac{1}{g_t^{\alpha}} + \frac{1}{2}\left(\frac{1}{g_i^{\alpha}} + \frac{1}{g_j^{\alpha}}\right), \tag{24}$$

where g_i^{α} is the conductance of phase α in pore i, g_j^{α} is the conductance in pore j, and g_t^{α} is the conductance of the connecting throat.

4.3.1 Conductance of the phases

The conductance of a pore or throat completely filled by one phase is assumed to be given by Poiseuille's Law,[4]

$$g = \frac{\pi r_{eff}^4}{8\mu_{\alpha} l}, \tag{25}$$

where $r_{eff} = \sqrt{A/\pi}$, μ is the viscosity of the phase, and A is the cross-sectional area of the pore or throat ($A = 4r^2$ for a square cross-section).

For two phases in a pore, the conductance of the wetting phase in the corners of the pore space (i.e. the water in Fig. 2) is approximated by an expression from Ransohoff and Radke.[42]

$$g^w = \frac{A_w r_{nw}^2}{R_f \mu_w l}, \tag{26}$$

where A_w is the cross-sectional area of the water, r_{nw} is the NAPL/water interfacial curvature, and R_f is a dimensionless resistance factor that has been tabulated.[42] Note that if we let $A_w = \pi r_{nw}^2$, the expression is similar to eqn. (25). The conductance of the non-wetting phase in the center of the throat is given by eqn. (25), except that the effective radius $r_{eff} = \sqrt{V_n/L\pi}$, where V_n is the volume of nonwetting fluid in the throat. For a pore use $r_{eff} = \sqrt{V_n/2\pi r_p}$.

The value of R_f depends on the boundary condition at the fluid interface and the contact angle. If the interface is immobile, the phases move independently and the relative permeability of one phase is not affected by flow of the others. This is a reasonable approximation for crude oil/water systems, where long carbon chain hydrocarbons and surfactants in the oil collect on the interface and render it immobile. For this case, $R_f = 248{\cdot}8$ for a square throat and a zero contact angle.[42] However, when clean fluids or gas contact the wetting phase in the corner, the interface can move. If we assume that there is no stress at the interface, $R_f = 93{\cdot}93$.[42] This is appropriate for gas/water and gas/NAPL interfaces. The values for R_f used in the network simulations are given in Table 4.

If there is no slip or partial slip at the fluid interface and the interface is mobile, then the flow of one phase affects the others. This leads to so-called cross-terms in the relative permeabilities, where the pressure gradient in one phase can cause flow in another. For two phase flow, this issue has been discussed by Kalaydjian.[23] We will show that consideration of the appropriate interfacial boundary conditions are extremely significant for three phase flow, when flow in NAPL layers occurs.

For three phases existing in a pore or throat, the conductances for the water and gas are given by eqns (26) and (25) respectively, and $r_{eff} = \sqrt{V_g/L\pi}$. We present three expressions for the conductance of a NAPL layer that lead to different functional forms of the relative permeability at low saturation.

(1) Free boundaries. The free boundaries case occurs if we assume that in every pore and throat all three phases are flowing with the same imposed potential gradient. Then NAPL and water together flow as an apparent single phase with a no stress boundary between the phases. We assume that the NAPL and water viscosities are equal ($\mu_n = \mu_w$). Thus the conductance of the NAPL is the conductance of the wetting layer of water and the NAPL together less the water conductance, or,

$$g_{ij}^n = \frac{(A_n + A_w)r_{gn}^2}{R_f^2 \mu_n l} - \frac{A_w r_{nw}^2}{R_f^1 \mu_w l}, \tag{27}$$

Table 4. Values used in network model simulations for the two different cases. All interfacial tensions are in mN/m. Note that different values for the resistance factor may be used depending on the number of phases in the particular pore or throat

Case	γ^e_{gw}	γ^e_{nw}	γ^e_{gn}	θ_{gn}	R_c	R_f (2 phases)	R_f (3 phases)
$C_s^{eq} = 0$	70	45	25	0°	1	93·93	93·93
$C_s^{eq} = -4$	66	45	25	33°	0·297	93·93	485

where A_n is the NAPL cross-sectional area and R_f is the resistance factor for a wetting fluid of contact angle θ in a corner. $R_f^1 = R_f^2 = 93{\cdot}93$ for a square corner and zero contact angle, while for instance if $C_s^{eq} = -4\,\text{mN/m}$ and $\gamma_{gn} = 25\,\text{mN/m}$, then from eqn. (9), $\theta_{gn} = 33°$ and $R_f^2 = 485$ ($R_f^1 = 93{\cdot}93$ as before since $\theta_{nw} = 0$).[42]

(2) Hydraulic radius approximation. The hydraulic radius approximation assumes a Poiseuille-type expression (eqn. (25)) for the conductance,

$$g_{ij}^n = \frac{A_n^2}{8\pi\mu_n l} \tag{28}$$

where A_n is the cross-sectional area of NAPL. This implicitly implies no slip at the boundary, but assumes that rather than being in a thin layer, the NAPL flows as though it occupies the center of a cylinder of area A_n. This is the expression that Lenormand and Zarcone[27] and Nilsen *et al.*[34] used for flow of a wetting phase in corners of the pore space.

(3) Film flow approximation. This case assumes that the water is treated as if it were a solid phase. Here, the NAPL/gas interface can either be a no stress or no slip boundary. In this case, expressions for g^n for various r_{gn} and r_{nw} may be found from Ransohoff and Radke[42] by using their expressions for wetting phase flow in a rounded corner. This is a good approximation for crude oil systems or if the water is stationary.

Approximation (1) will be used in all the results presented here, although this will tend to over-estimate the NAPL conductance if flow in layers is significant.

Note that we assume that the pressure gradient in one phase has no effect on the flow rate of any other phase. Thus, although we consider the interfacial boundary conditions, we do not allow cross terms in the relative permeability. The determination of relative permeability cross terms is beyond the scope of this work.

4.3.2 Calculating the relative permeability

The relative permeability of a given phase in the network model is calculated as follows:

1. A section of pores in the network model is selected upon which the calculation of relative permeability will be used. For the results presented below, the calculations were performed on a $15 \times 15 \times 15$ section, which was the last half of a $30 \times 15 \times 15$ network model (flow is in the x-direction). A section of the network away from the inlet phase is used to avoid inlet boundary effects.
2. The saturation of the desired phase in the last half of the network model is calculated using the method described in Section 4.2.
3. The conductance in each pore and throat for the phase is determined using the proper expressions as described in Section 4.3.1. To determine the absolute permeability, the single phase expression for conductance in pores and throats is used.
4. The conductance between connecting pores is determined using the harmonic mean (eqn. (24)).
5. Constant pressure boundary conditions are placed on each side of the section of interest.
6. Equation (22) is written for each pore using eqn. (23) for the flow rate between each pore. A set of equations is then created with a matrix that contains the conductances between pores. The pressures of each pore are unknowns and the right hand side contains the conductances between the network section and the boundary.
7. The set of equations are solved using an iterative conjugate gradient solver with incomplete Cholesky preconditioning. This determines the pressures of the pores.
8. Given the pressures of the pores, the flow rates for the phase in and out of the section of the network model can be determined using eqn. (23).
9. Given the total flow into or out of the section of the network, the phase viscosity, the imposed pressure drop, and the absolute permeability, the multiphase Darcy's law (eqn. (2)) is applied to determine the relative permeability of the phase at the calculated saturation.

Let us recap on the approximations we have made to compute relative permeability. (1) We assume Poiseuille-type flow. This is a good approximation for slow flow in porous media. (2) We use simplified interfacial boundary conditions which ignore the effect of the flow of one phase on the flow of the others. This may be a poor approximation in some cases, but does allow us to describe the different types of possible behavior. (3) If a phase is not connected from one side of the $15 \times 15 \times 15$ network to another its relative permeability is zero. Water is always connected, but gas and NAPL can be trapped. However, double displacement can mobilize trapped phases and thus, since the phase is displaced, the true relative permeability may be finite even if a phase is not continuous. This issue will be discussed later.

We present results for a $30 \times 15 \times 15$ grid. We ran several cases on a $40 \times 20 \times 20$ grid and found no

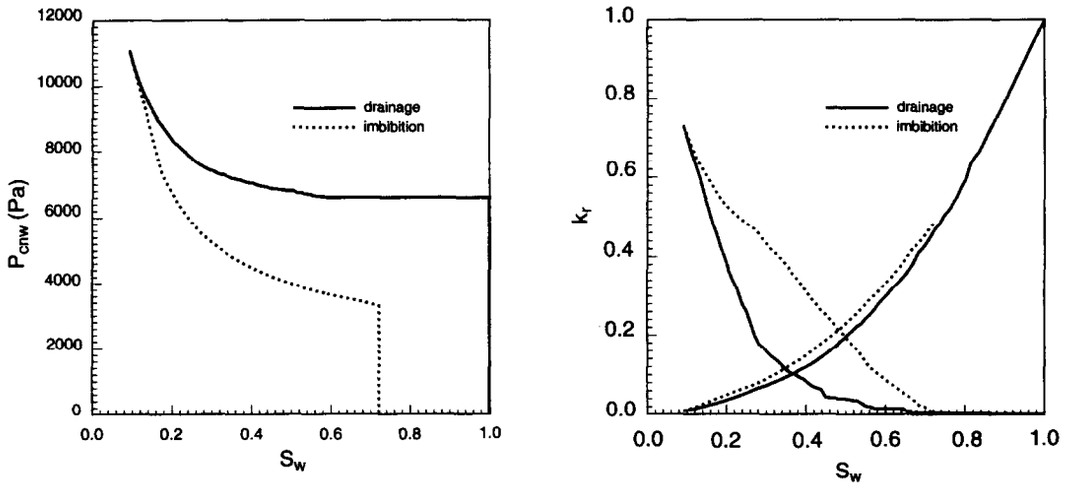

Fig. 11. Two phase capillary pressure and relative permeability curves. The relative permeability curves are characteristic of unconsolidated sand.

significant differences in the results. For every case we ran at least two realizations and again we found no difference between realizations. For clarity, we only present results for a single realization in the paper. Diaz *et al.*[10] found that a 15 × 15 × 15 network was sufficient to reproduce satisfactory capillary pressure curves.

5 RELATIVE PERMEABILITY

5.1 Two phase relative permeability and capillary pressure

Figure 11 shows capillary pressure and relative permeability curves simulated for NAPL/water flow. The network is originally fully saturated with water. Then NAPL invades the network (drainage) and the capillary pressure increases. At a water saturation of slightly less than 10%, NAPL invasion is stopped. Water then invades the system (imbibition) and the capillary pressure decreases. The expressions in Section 3 are used to compute threshold pressures for snap-off and piston-like advance. For pore filling, $P_c = 1{\cdot}8\gamma_{nw}/r_{nw}$ for I_1, and $P_c = 1{\cdot}25\gamma_{nw}/r_{nw}$ for I_2. Note that the C_{I_1} and C_{I_2} constants have been selected arbitrarily. I_3 and higher mechanisms are not allowed. NAPL may only be displaced if it is connected from the inlet face to the outlet. Snap-off allows NAPL to be trapped, and for this displacement the residual NAPL saturation is 28%.

No attempt was made to match experimental data exactly, but the capillary pressure and relative permeability curves are representative of those for unconsolidated sand with a relatively narrow pore size distribution.[12,30,33] However, when compared to experimental measurements of relative permeability for unconsolidated sands, the nonwetting phase relative permeability values appear to be too low. This is caused by the method in which saturation is calculated, which tends to overestimate the volumes in the pores compared to the throats due to the simplified geometry of the network model. Previous work has provided corrections to the saturation calculation.[19,21,32] We have not adjusted the saturation calculations.

5.2 Routes in capillary pressure space

Figure 12 is a schematic diagram representing different three phase displacements as paths in $P_{cgn} - P_{cnw}$ space. All NAPL/water two phase displacements occur on the P_{cnw} axis. When gas is introduced into the system, P_{cgn} becomes defined and finite. The line denoted by $R = R_c$ separates the region where NAPL layers are stable from the region where NAPL layers do not exist. The value for R_c is calculated using eqn. (10). Table 4 gives the values for R_c for the cases investigated. We shall examine two different displacements representing the paths BCD and AD. The final capillary pressures for both displacements are the same.

Let B in Fig. 12 represent a two phase NAPL/water system at a high capillary pressure corresponding to high NAPL saturation. This condition could represent a large NAPL spill that has depressed the water table. If the water table is subsequently lowered, air will invade into the system, creating three phase flow. Eventually, point C will be reached, and a certain amount of NAPL would be displaced. The BC path might have a large portion of three phase flow occurring in the region where NAPL layers are stable. Since the NAPL cannot be trapped when layers exist, the BC path may result in very high recovery. If the water table rises again, three phase imbibition occurs, reducing P_{cnw} to point D. This imbibition process may also result in increased NAPL recovery due to double imbibition displacements.

If the system is at point B and the water table rises, P_{cnw} can be lowered to A, where the NAPL is found only in disconnected ganglia. If air invades into the NAPL

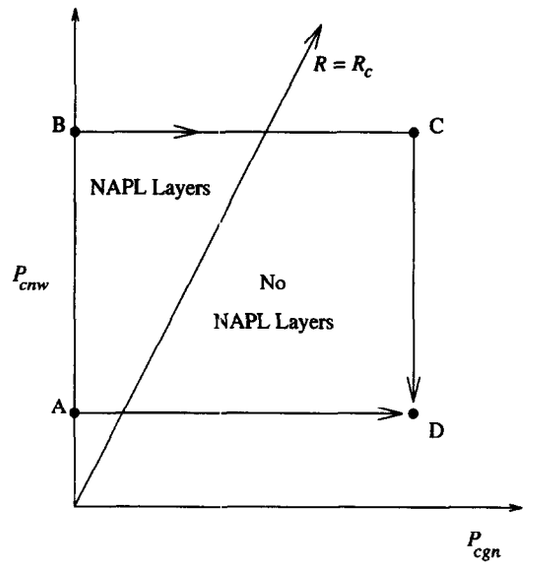

Fig. 12. Different paths in capillary pressure space. The $R = R_c$ line separates the regions of NAPL layer stability. Path BCD represents gas invasion into high P_{cnw} corresponding to high S_n, followed by imbibition of water. Path AD represents gas invasion into low P_{cnw} corresponding to residual NAPL saturation after water invasion.

and water through the lowering of the water table to D, the majority of the displacement would occur in the region where NAPL layers are not stable, and the disconnected NAPL could only be displaced through double drainage.

At point D, the capillary pressures for both sequences of displacements would be the same. Yet before any actual results are calculated, we can already imagine that the residual NAPL saturations and the relative permeabilities can be drastically different. We now present results for two different cases, one where $C_s^{eq} = 0$, representing a system with a positive initial spreading coefficient such as air/Soltrol/water, another where $C_s^{eq} = -4$ mN/m, representing a nonspreading system such as air/*n*-decane/water.[20]

5.3 $C_s^{eq} = 0$ case — results

The network initially contains water only. Drainage to approximately 90% NAPL and 10% water proceeds as described in Section 5.1. The two different routes in capillary pressure space sketched in Fig. 12 are then followed. Table 4 gives the values used in the simulations.

Figure 13 shows the capillary pressure path and the corresponding saturation path with $C_s^{eq} = 0$ for the three phase displacements described above. Table 5 indicates the saturation values for the simulations corresponding to the paths indicated in Fig. 12. The solid line in Fig. 13 represents path BC. Gas invades into 10% water and 90% NAPL holding P_{cnw} constant at its maximum value. All the NAPL is recovered for this

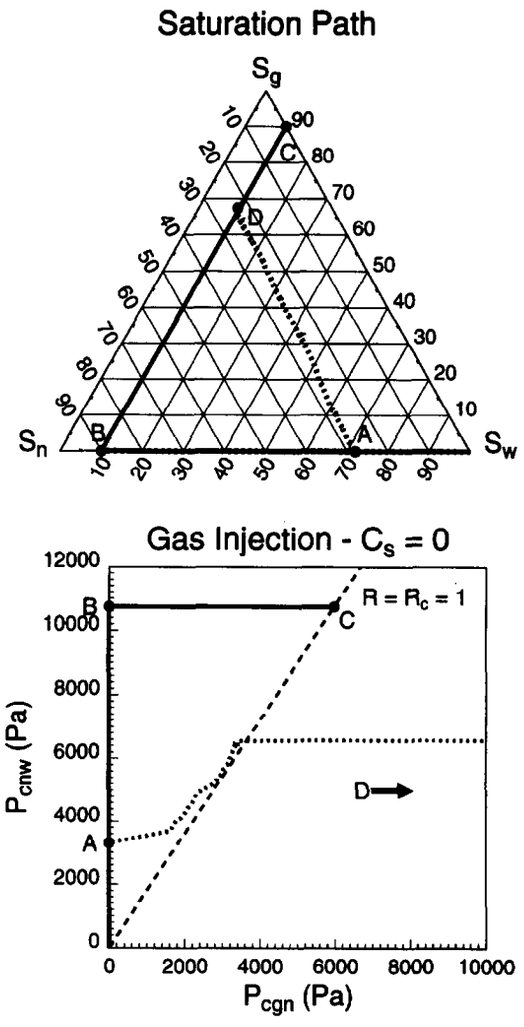

Fig. 13. Capillary pressure and saturation paths for displacements occurring at $C_s^{eq} = 0$. The solid line represents gas invasion into 90% NAPL and 10% water. All of the NAPL is recovered for this case. The dashed line represents invasion of gas into residual (28%) NAPL and water. Here, an additional 5% of NAPL is recovered from gas invasion after the NAPL is disconnected. The capillary pressure for point D is off the scale.

case. Before the gas enters the network, the NAPL is continuous. P_{cnw} is determined by the smallest throat invaded by NAPL. When gas is introduced into the system, NAPL layers are stable and thus the NAPL stays continuous. For $C_s^{eq} = 0$, the point at which NAPL layers disappear ($R = R_c = 1$) also corresponds to the P_{cgn} necessary for the gas to enter the smallest NAPL-filled throat. Thus the gas can displace all of the NAPL while NAPL layers are stable, resulting in 100% recovery. Clearly, this is the ideal case. The route CD in Fig. 12 would not alter the NAPL saturation since there is no NAPL to displace.

The AD path is represented by the dashed line in Fig. 13. Before gas invades into the network, water is allowed to imbibe into the NAPL until all the NAPL is trapped with a residual saturation of 28%. Gas is then

Table 5. Saturation values at the start and end points of the capillary pressure paths demonstrated in Fig. 12. Note that the CD path for the $C_s^{eq} = 0$ case was not taken

	Start point			End point		
Path	S_n	S_w	S_g	S_n	S_w	S_g
$C_s^{eq} = 0$						
BC	0·90	0·10	0·0	0·0	0·10	0·90
CD	—	—	—	—	—	—
AD	0·28	0·72	0·0	0·23	0·09	0·68
$C_s^{eq} = -4$ mN/m						
BC	0·90	0·10	0·0	0·42	0·02	0·56
CD	0·42	0·02	0·56	0·42	0·04	0·54
AD	0·28	0·72	0·0	0·24	0·08	0·68

introduced into the network model. For this displacement, NAPL layers become unstable at a much lower P_{cgn}, before any significant amount of NAPL is displaced. P_{cnw} is defined as the lowest pressure before the NAPL is disconnected during imbibition. When gas is injected, double drainage reconnects the NAPL briefly. P_{cnw} then rises, as shown. The incremental NAPL recovery, which is merely 5% in this case, is due solely to double drainage unaided by NAPL layer flow. The final residual NAPL saturation of 23% occurs when P_{cgn} reaches over 85 kPa, which is off the scale in Fig. 13.

Figure 14 shows the configuration of water and residual NAPL before gas injection in a two-dimensional network which visually reproduces the same behavior as our three-dimensional simulation. Figure 15 shows the distribution of gas, NAPL and water at gas breakthrough, while Fig. 16 shows the fluids at the end of gas injection when the NAPL is trapped and water is only contained in wetting layers. Note that double drainage re-arranges the NAPL distribution — the NAPL is

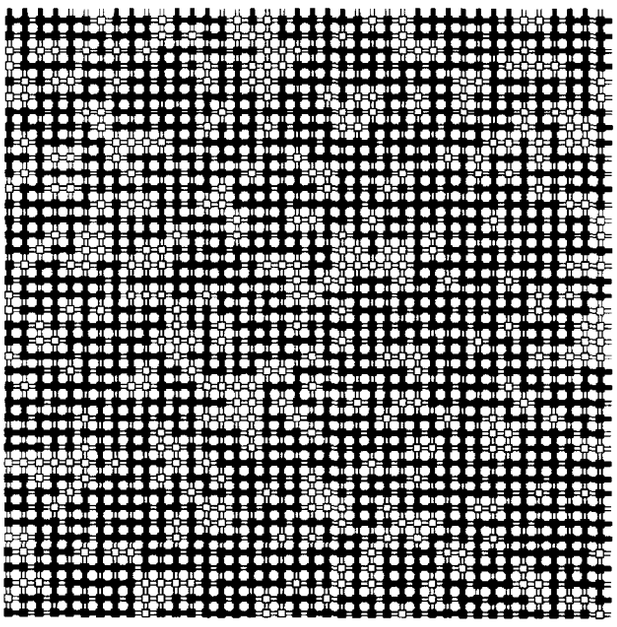

Fig. 14. The configuration of residual NAPL (black) and water (clear) in a two-dimensional 40 × 40 network.

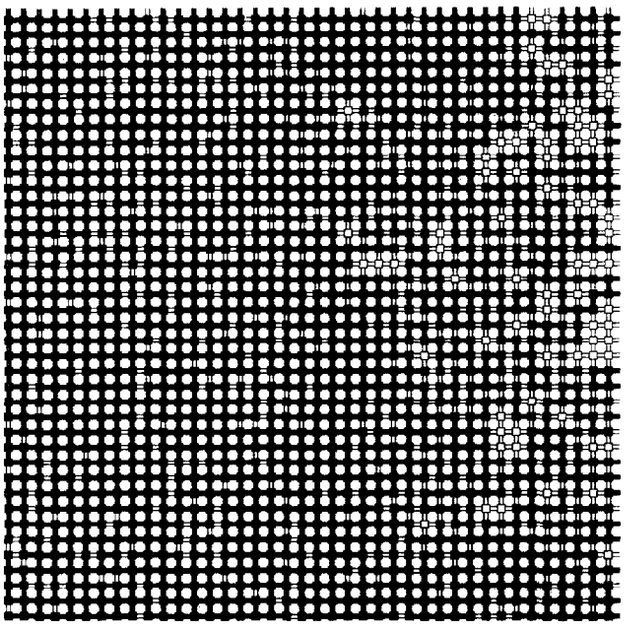

Fig. 15. The configuration of NAPL (black), gas (grey), and water (clear) in a two-dimensional 40 × 40 network at gas breakthrough.

displaced from the largest pores and throats and tends to reside in clumps, rather than have a dendritic or tree-like structure shown in Fig. 14. Note that Figs 15 and 16 show a high degree of NAPL displacement from the inlet section of the network. This is caused by two factors: end effects at the inlet section, and NAPL layers. The end effects are similar with what one would see in a micromodel. A high gas saturation accumulates close to the inlet, causing a large amount of NAPL to be displaced. In addition, at the beginning of the displacement before gas breakthrough, NAPL layers are present. This allows the NAPL to be displaced near the inlet and there is no trapping. When the value of R (eqn. (6)) exceeds the critical ratio R_c (eqn. (10)), the layers disappear and the NAPL can be trapped by gas.

The water relative permeability (k_{rw}) curve for the case where gas invades into water and residual NAPL (path AD) is shown in Fig. 17 and is similar to the two phase k_{rw} shown in Fig. 11. For the case representing path BC, the NAPL is displaced preferentially to the water, resulting in a constant water saturation throughout the entire displacement. The water relative permeability for this displacement is a constant value of 0·0106 shown in Fig. 17.

The gas relative permeabilities are plotted in Fig. 18 with the points of the different capillary pressure paths indicated. For gas invasion into 90% NAPL, the relative permeability is similar to the nonwetting curve in two phase drainage. This is because gas is nonwetting and NAPL and water combined behave as the wetting phase. The configuration of gas is similar to the pattern of NAPL shown in Fig. 14 except, of course, that the gas is connected. In particular, the gas has a dendritic

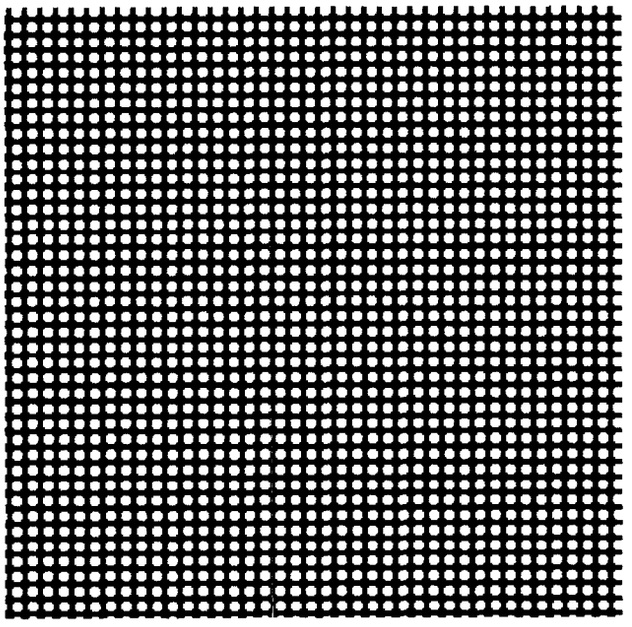

Fig. 16. The configuration of residual NAPL (black), gas (grey), and water (clear) in a two-dimensional 40 × 40 network at the end of gas injection. The water only exists in wetting layers and is not shown.

structure with a relatively low conductance. However, k_{rg} for gas injection into residual NAPL is higher. Here, NAPL layers are not stable for most of the displacement and NAPL does not appear to be completely wetting in the presence of gas. k_{rg} is higher because the gas occupies connected channels in the pore space, similar to those illustrated in Fig. 16, which have a higher conductance than the dendritic structure of the nonwetting phase in drainage. Note, though, that the relative permeability values are low, which is an artifact of the saturation calculation mentioned earlier when discussing two phase flow.[21,32]

Figure 19 shows the NAPL relative permeabilities, which show significant hysteresis. For gas into 90% NAPL, the relative permeability is finite down to $S_n = 0$. k_{rn} at low NAPL saturation is due to flow in NAPL layers and will be discussed in more detail in Section 6. For gas into residual NAPL, where NAPL layers are not stable, NAPL may be trapped. k_{rn} starts and ends at zero, but is finite when double drainage reconnects the NAPL. k_{rn} for gas into residual NAPL is nonzero only when the NAPL is connected, even though there is some displacement to lower NAPL saturations through double drainage. For this case, k_{rn} is erroneously calculated. Since double displacements are entirely capillary controlled, they cannot preferentially transport fluid in

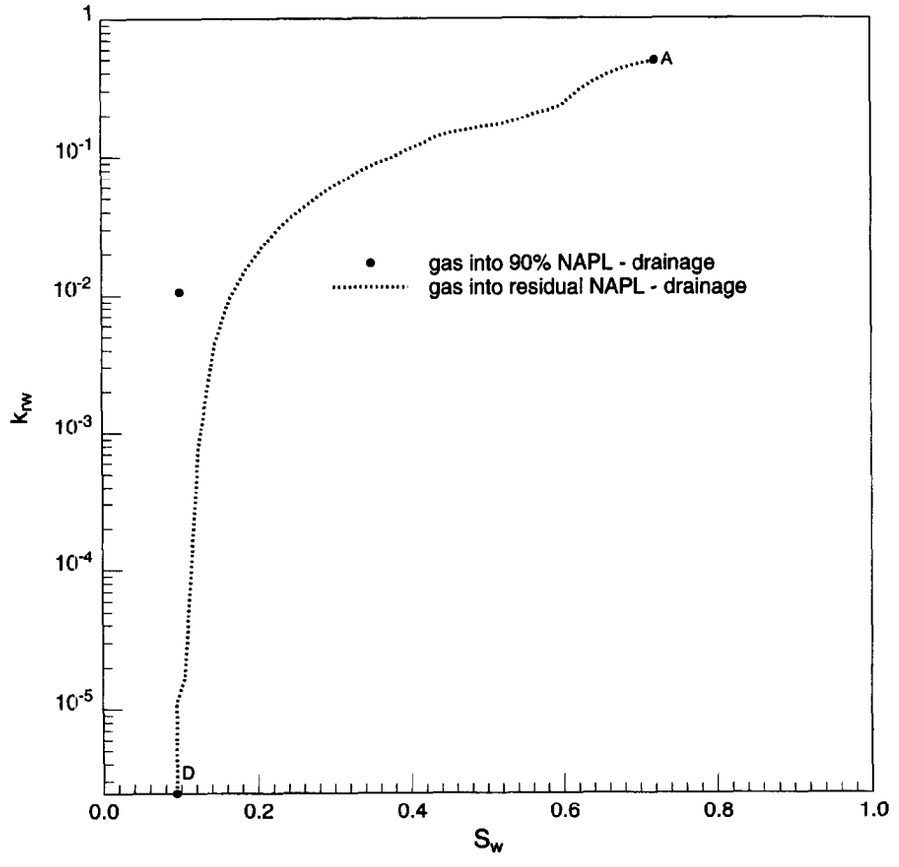

Fig. 17. Water relative permeability for $C_s^{eq} = 0$ displacements. Gas invasion into 90% NAPL does not displace any water, so the relative permeability is simply a constant value for that displacement.

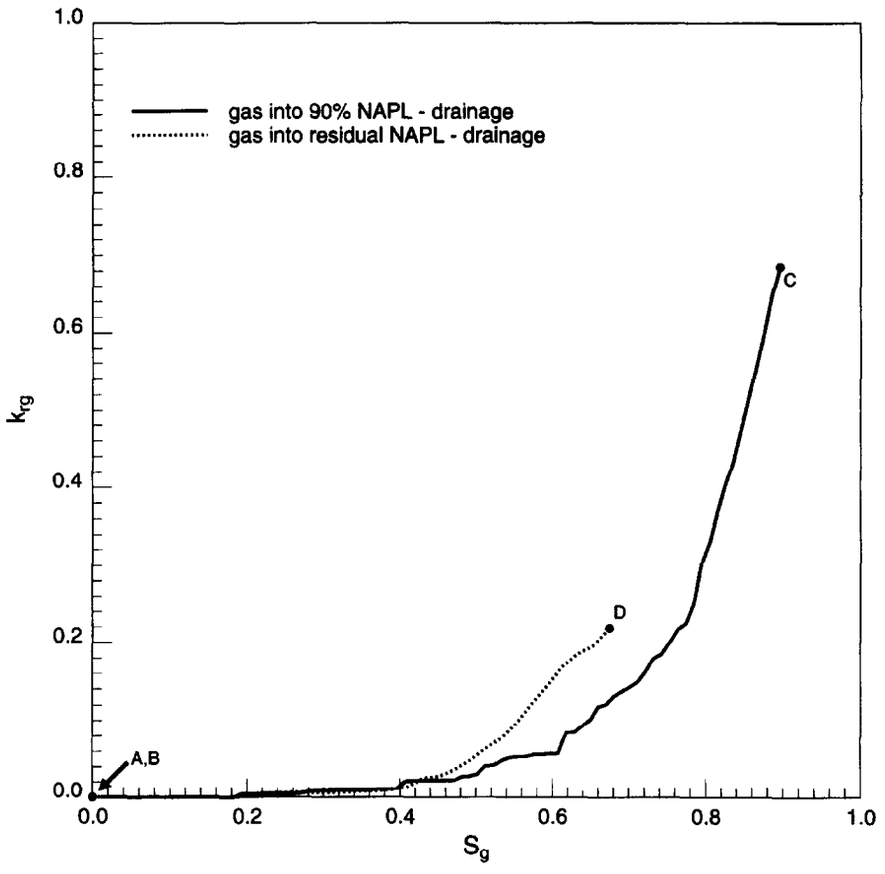

Fig. 18. Gas relative permeability for $C_s^{eq} = 0$ displacements. Even for two drainage situations, the gas relative permeability can vary. The curve for gas invasion into 90% NAPL mimics the two phase drainage NAPL relative permeability curve.

any direction. Double drainage simply rearranges the fluids in the pore space. Thus, double drainage must, in a sufficiently large system, cause the NAPL to reconnect (enabling $k_{rn} > 0$) for there to be any decrease in NAPL saturation. We did observe this, but the continued displacement of disconnected NAPL is an artifact of the small networks we used and the fact that we allowed no NAPL to enter the inlet face during gas injection.

5.4 $C_s^{eq} = -4$ mN/m case — results

Figure 20 shows the same two displacements illustrated in Fig. 13, except that the displacements are with a nonspreading system with $R_c = 0{\cdot}297$, which means that NAPL layers are only stable for a very restricted range of capillary pressures. Refer to Table 5 for the start and end point saturations for the capillary pressure paths considered below.

The displacement of 90% NAPL by gas (path BC) no longer recovers all the NAPL. 42% of the NAPL remains trapped by both gas and water, which is a poorer recovery from injecting water alone. When gas invades NAPL and NAPL layers do not exist, it is unable to form loops in the pore space. When gas attempts to connect two gas-filled portions of the network, it must first displace a disconnected region of NAPL. This is impossible, and thus the gas is forced to maintain a poorly connected dendritic structure. Gas can only form loops by displacing water. This phenomenon leads to a very low k_{rg} and significant trapping of NAPL in both pores and throats. This issue is discussed for two phase flow in more detail by Blunt *et al.*[5] The rise in P_{cnw} occurs when the NAPL becomes disconnected and then reconnects by double drainage. After gas injection, water invades the system (path CD) and P_{cnw} is reduced (off the scale in Fig. 20). The gas rapidly becomes disconnected by snap-off with an increase of S_w of only 2%. Double imbibition does occur, but in this example it displaces an insignificant amount of NAPL.

Injection of gas into water and residual NAPL (path AD) recovers nearly the same amount of NAPL (4%) by double drainage as when $C_s^{eq} = 0$.

For these displacements we have hysteresis in the relative permeabilities for NAPL, water, and gas. From Fig. 21 it is apparent that k_{rw} depends on saturation history for negative spreading coefficients. At low water saturation, the water resides principally in wetting layers in the corners of the pore space. For $C_s^{eq} < 0$, the NAPL/water and gas/water interfaces in the corner have different radii of curvature, and hence a NAPL-fitted throat has a different water saturation and conductance than a gas-filled throat. The overall water

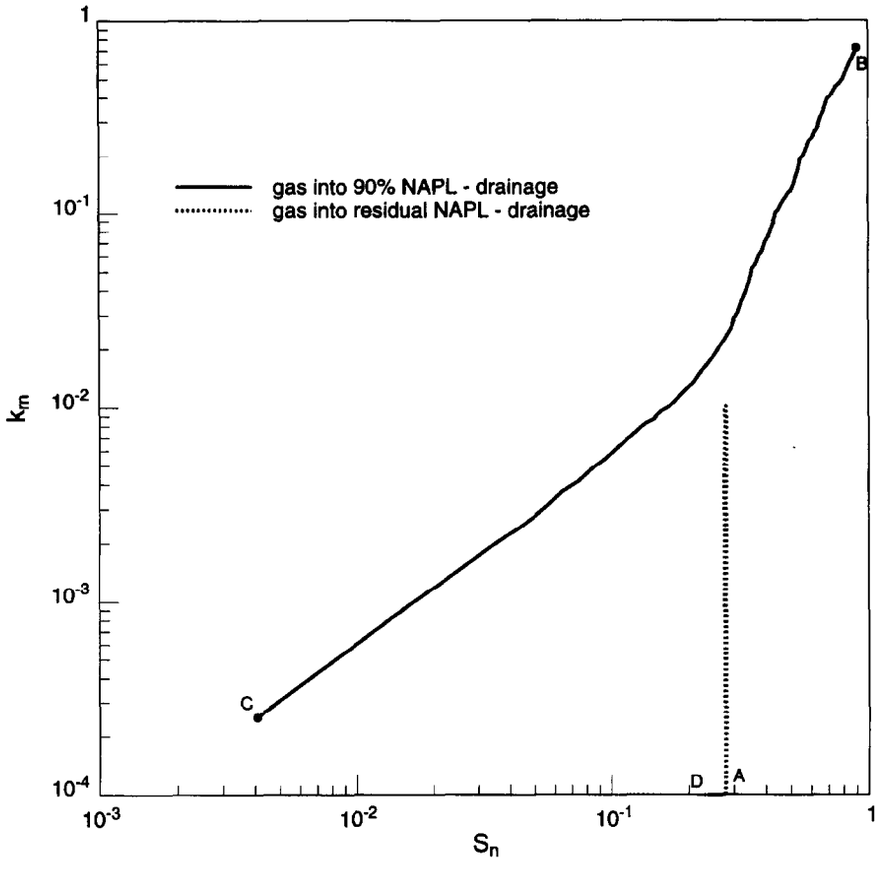

Fig. 19. NAPL relative permeability for $C_s^{eq} = 0$ displacements. For gas invasion into 90% NAPL, the NAPL relative permeability is finite down to a NAPL saturation of zero (curve extending to zero saturation not shown). The relative permeability at low saturations is due to flow in NAPL layers. For gas invasion into water and residual NAPL, the relative permeability is finite only when the NAPL is reconnected.

conductance is thus a function of both NAPL and gas saturations.

Figure 22 shows that k_{rg} for gas into residual NAPL is similar to that for $C_s^{eq} = 0$, but k_{rg} for gas into 90% NAPL is up to 100 times lower, because the gas is forced to have a very dendritic structure with very few connected loops. The curves are not smooth, particularly at low gas saturation, because of the finite size of the network. As mentioned previously, the k_{rg} curves may change if the saturation calculations were adjusted.

Figure 23 shows k_{rn} for the two cases with $C_s^{eq} = -4\,\text{mN/m}$. k_{rn} for gas into residual NAPL is again similar to that for $C_s^{eq} = 0$, but for gas into 90% NAPL, the relative permeability falls to zero when $S_n \approx 42\%$, indicating the large degree of trapping.

5.5 Effect of spreading coefficient and initial water saturation on residual NAPL saturation

The previous section revealed how the value of the spreading coefficient and the amount of water in the network could influence the ultimate recovery of NAPL. In this section we investigate further the effect these parameters have.

5.5.1 C_s^{eq} vs S_{nr}

The two possible types of pore level displacements that can occur when gas invades into water and trapped NAPL are double drainage and direct gas → water. Let us make a simple comparison of the threshold capillary pressures for the two mechanisms. The double drainage threshold capillary pressure is given by eqn. (14). The threshold capillary pressure for the gas → water displacement is $P_{c_{gw}} = 2\gamma_{gw}^e / r_{gw}$. If we substitute eqn. (9) for $\cos\theta_{gn}$ into eqn (14) and assume that all the radii of curvature are the same, we find that the threshold capillary pressures are equal when $\gamma_{gw}^e = \gamma_{nw}^e + \gamma_{gn}^e + C_s^{eq}$, which is always true (eqn. (4)). Thus for any value of C_s^{eq}, neither double drainage or gas → water are favored over the other if the radii of curvature are equivalent. Double drainage therefore is favored only when the NAPL is displaced through larger pores and throats than direct gas → water.

A series of displacements at varying values of C_s^{eq} were performed in order to test the effect of C_s^{eq} on NAPL recovery. The network model initially contained water. NAPL was allowed to invade into the network up to 85% saturation. Water then displaced the NAPL until the residual NAPL saturation was reached, at which point all the NAPL was disconnected. Gas was

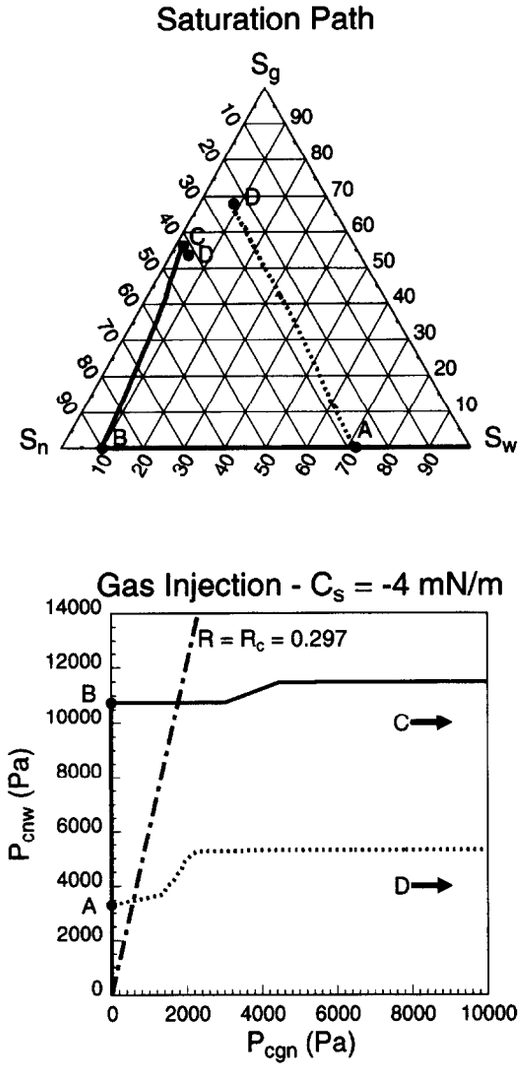

Fig. 20. Capillary pressure and saturation paths for displacements occurring at $C_s^{eq} = -4\,\text{mN/m}$. The solid line represents gas invasion into 90% NAPL and 10% water. The dashed line represents invasion of gas into residual (28%) NAPL and water. Over 45% of the NAPL remains in the network after gas invasion for the first case, whereas gas invasion into trapped NAPL results in 24% residual NAPL after gas invasion is complete. The capillary pressures for points C and D are off the scale.

subsequently injected into the network until no more NAPL was displaced. A $20 \times 15 \times 15$ network model with a slightly wider pore and throat size distribution than previously was used, and the saturation of the entire network is presented.

The value of C_s^{eq} had no discernable effect on the residual NAPL saturation after gas invasion. The residual NAPL saturation after water injection was 33%. A further 10% of NAPL was recovered beyond the residual NAPL saturation to water alone.

Since imbibition occurs in the smallest pores and throats in the pore space, at the end of imbibition the trapped NAPL will be found only in the larger pores and throats. For the pore and throat size distributions we studied, double drainage is favored over gas → water for a large range of spreading coefficients. Thus the value of C_s^{eq} may have little effect on the recovery of trapped NAPL after water invasion. Double drainage rearranges the NAPL distribution and results in a large incremental recovery for systems with a wide range of pore and throat sizes.

5.5.2 S_{wi} vs S_{nr}

The previous displacements representing paths BC and AD results in drastically different residual NAPL saturations. A series of displacements were performed to determine how the initial water saturation (S_{wi}) when gas first invades the network influences the residual NAPL saturation after gas injection is complete.

The network again initially contains only water. NAPL is allowed to invade the network up to 99% saturation. Water is allowed to re-invade the network until the desired S_{wi} is obtained. Gas is subsequently injected until all the NAPL is trapped. The procedure is repeated for $C_s^{eq} = 0$ and $C_s^{eq} = -4\,\text{mN/m}$. A $20\times$ 15×15 network is again used with the same distributions as the previous section, and the saturations of the entire network are calculated.

Figure 24 gives the results of the network model runs. The saturation of water when gas is injected greatly affects the residual NAPL saturation (S_{nrg}) after gas injection is complete. Note that for some values of S_{wi}, S_{nrg} is larger than the trapped NAPL saturation after water invasion S_{nrw}. This demonstrates how the competition for pore space between gas, NAPL, and water can limit the recovery of NAPL.

For this particular case, NAPL layers are stable throughout the displacement for $C_s^{eq} = 0$ when the initial NAPL saturation is greater than approximately 80%. For initial NAPL saturations at 80% and higher with $C_s^{eq} = 0$, all the NAPL is recovered during gas injection. However, for $C_s^{eq} = -4\,\text{mN/m}$, NAPL layers are not stable throughout the displacement and NAPL recovery is lower.

6 NAPL RECOVERY RATE

The previous section demonstrates that the ultimate recovery of NAPL can be very high in the presence of water and gas. However, the rate of NAPL recovery has not yet been discussed. Experimental work on sand columns by Blunt *et al.*[6] and Zhou and Blunt[52] found very high recoveries of NAPL in sandpacks down to 0·1%. These experiments took approximately three weeks to perform. However, work performed by Dumoré and Schols[14] on consolidated rock required over 3 months for NAPL saturations to reach 3%. Skurdal *et al.*[45] were also required to wait for $1\frac{1}{2}$ to 3 months to see NAPL saturations in their experiments

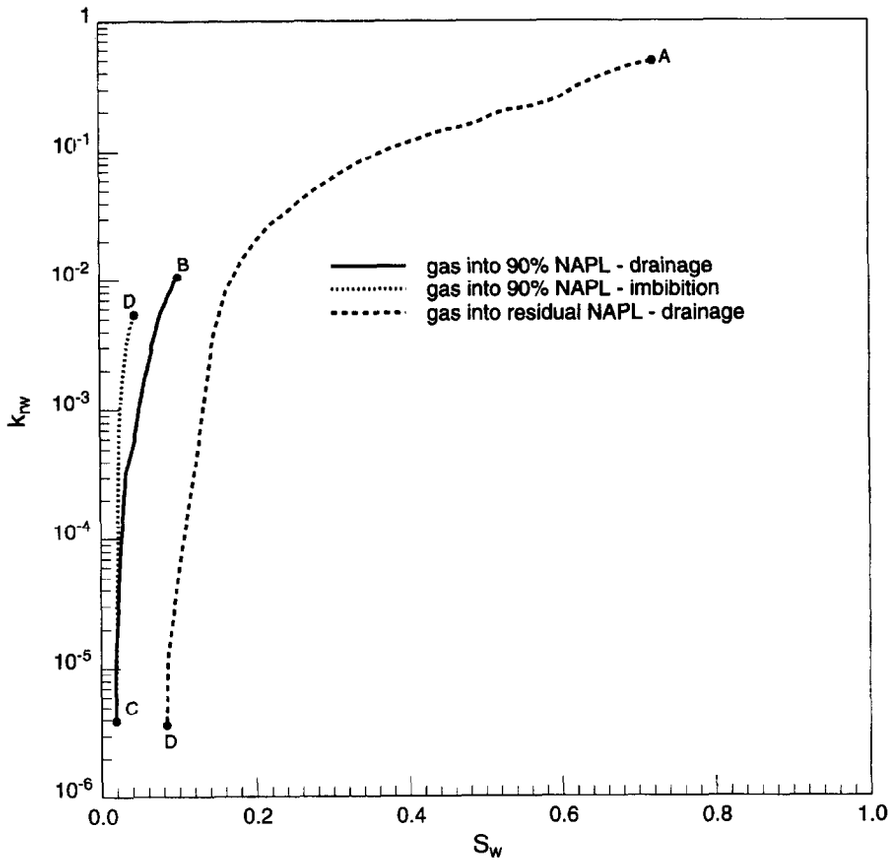

Fig. 21. Water relative permeability for $C_s^{eq} = -4\,\text{mN/m}$ displacements. The relative permeabilities demonstrate significant hysteresis for each case due to the differing radii of curvature of the water layers in the corners.

reach 5%. This section provides a simple analysis of the rate of NAPL recovery down to very low saturations.

Consider one-dimensional vertical flow of NAPL whose only driving force is gravity. If eqn (2) holds, the mass balance equation is,

$$\phi\frac{\partial S_n}{\partial t}+\frac{\partial}{\partial z}\left(\frac{Kk_{rn}\rho_n g}{\mu_n}\right)=0, \tag{29}$$

where ϕ is the porosity of the medium. Assuming $k_{rn}=k_{rn}(S_n)$ only, eqn. (29) can be manipulated into an equation with only a single variable. Substituting $v=z/t$, we obtain,

$$\frac{\partial S_n}{\partial v}\left(\frac{K\rho_n g}{\phi\mu_n}\frac{\partial k_{rn}}{\partial S_n}-v\right)=0. \tag{30}$$

The independent variable v represents the characteristic velocity of the NAPL saturation S_n. The solution to eqn. (30) is simply,

$$v=\frac{z}{t}=\frac{K\rho_n g}{\phi\mu_n}\frac{\partial k_{rn}}{\partial S_n}. \tag{31}$$

Equation (31) gives the characteristic velocity of recovery during gravity drainage. The time to reach a saturation S is given by,

$$t=\frac{\phi\mu_n z}{K\rho_n g(\partial k_{rn}/\partial S_n)}. \tag{32}$$

For the three boundary conditions mentioned in Section 4.3.1, k_{rn} at low S_n (when NAPL is only contained in layers) is quite different. For case (1) in Section 4.3.1, free boundaries, the expression of the conductance g^n (eqn. (27)) can be re-written in terms of the saturation in a single throat of radius r. We note that $A=4r^2$, and thus $S_n=A_n/4r^2$, $S_w=A_w/4r^2$ and $A_n=(4-\pi)(r_{gn}^2-r_{nw}^2)$, $A_w=(4-\pi)r_{nw}^2$, for a throat of square cross-section with $\theta_{gn}=\theta_{nw}=0$. Thus, after some algebra,

$$g^n=\frac{16r^4}{(4-\pi)R_f\mu_n l}(S_n^2+2S_nS_w). \tag{33}$$

A local relative permeability is the ratio of g^n to the conductance in a completely filled throat, which from eqn. (25) is $g=2r^4/\pi\mu l$. Thus, we expect

$$k_r\sim\frac{g^n}{g}=\frac{8\pi(S_n^2+2S_nS_w)}{(4-\pi)R_f}. \tag{34}$$

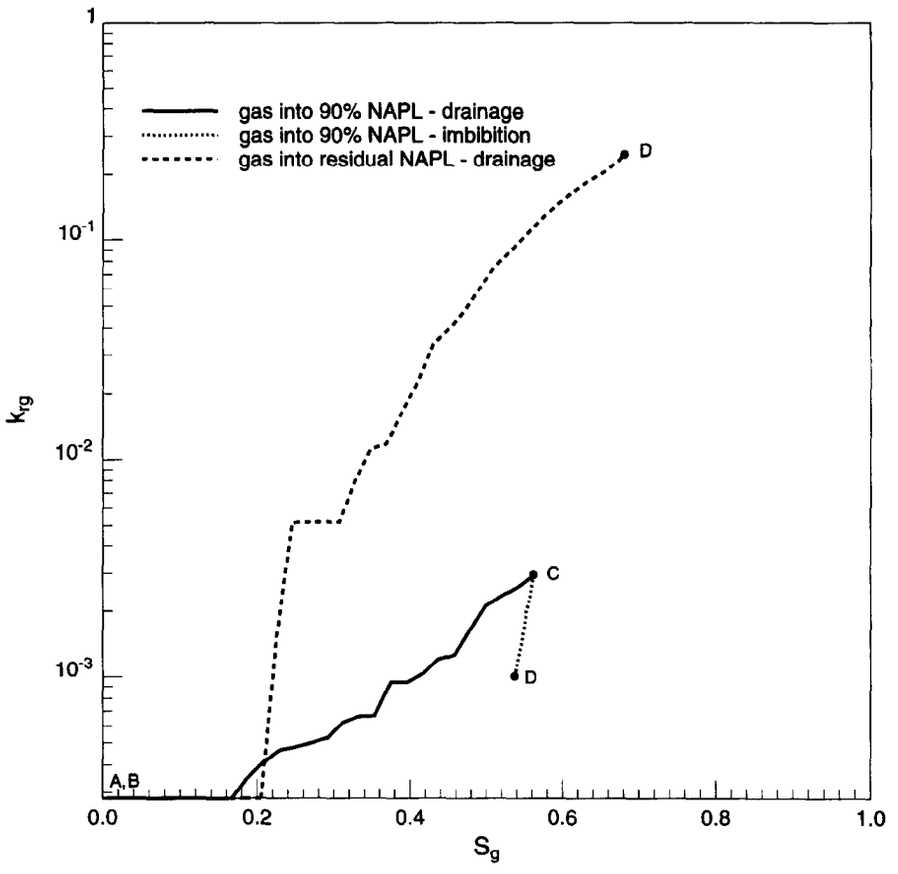

Fig. 22. Gas relative permeability for $C_s^{eq} = -4$ mN/m displacements. The gas invasion into 90% NAPL relative permeability curve is much lower than the gas invasion into residual NAPL curve. When NAPL layers are not stable, the NAPL prevents the gas from forming connected loops. High NAPL saturation thus causes the gas to have a highly dendritic structure and low conductivity.

For $S_n \ll S_w$ this gives $k_r \sim 0{\cdot}062 S_n$ for $R_f = 93{\cdot}93$ and $S_w = 0{\cdot}1$. The relationship is confirmed in Fig. 19 for gas injection into 90% NAPL when $C_s^{eq} = 0$. In Fig. 19, for $S_n < 0{\cdot}1$, $k_{rn} \approx 0{\cdot}06 S_n$.

For case (2), the hydraulic radius approximation, it can be shown that $k_{rn} \sim S_n^2$, and for case (3), film flow, $k_{rn} \sim S_n^3$ for fixed S_w.

It can be seen that for small NAPL saturations, the boundary condition at the NAPL/water and NAPL/gas interfaces has a dramatic effect on the relative permeability and hence drainage rates. An estimated minimum drainage time can be calculated using eqn. (32) and assuming $k_{rn} = 0{\cdot}06 S_n$. For the sand column work of Zhou and Blunt,[52] $K \approx 40\,\text{D} \approx 4 \times 10^{-11}\,\text{m}^2$, $\phi = 0{\cdot}4$, $\mu_n \approx 10^{-3}\,\text{Pa s}$, $\rho_n g \approx 8000\,\text{Pa s}^{-1}$, and $z = 1\,\text{m}$, then the drainage time $t \approx 6\,\text{h}$. If the experiments were performed in consolidated rock of $K \approx 500\,\text{mD} \approx 5 \times 10^{-13}\,\text{m}^2$, $\phi = 0{\cdot}2$, $t \approx 10$ days. These times are somewhat lower that the experimental values. Note, however, that the expression used for the conductance of NAPL layers most likely overestimates the real conductance of NAPL layers for these cases. For the case of a NAPL flowing in the vadose zone to the water table, $K \approx 1\,\text{D} \approx 1 \times 10^{-12}\,\text{m}^2$, $\phi = 0{\cdot}3$, and $z = 1\,\text{m}$, $t \approx 7{\cdot}3$ days. In a typical oil reservoir, $K \approx 100\,\text{mD}$ ($10^{13}\,\text{m}^2$), $\phi = 0{\cdot}2$, and $z = 50\,\text{m}$, the estimated minimum drainage time would be approximately 5·3 years.

7 DISCUSSION

The pore level configuration and displacement of three phases based on considerations of capillary equilibrium and observations from micromodel experiments have been studied. This analysis allows us to construct a rule-based three phase network model.

The relative permeabilities, especially for flow at low NAPL saturation, are sensitive to saturation pathway, the boundary conditions at the fluid interfaces, and the equilibrium spreading coefficient. None of these features are included in present empirical models.

We have computed NAPL recoveries and relative permeabilities for a specified route in capillary pressure space. However, we do not know this route *a priori* for a displacement with known initial and injection conditions. For instance, our studies have implied that the NAPL recovery for injection into residual NAPL is much lower than for injection into a high NAPL saturation. However, this is only true if P_{cnw} is maintained at a low value. In gravity drainage experiments, gas invasion into residual NAPL typically results

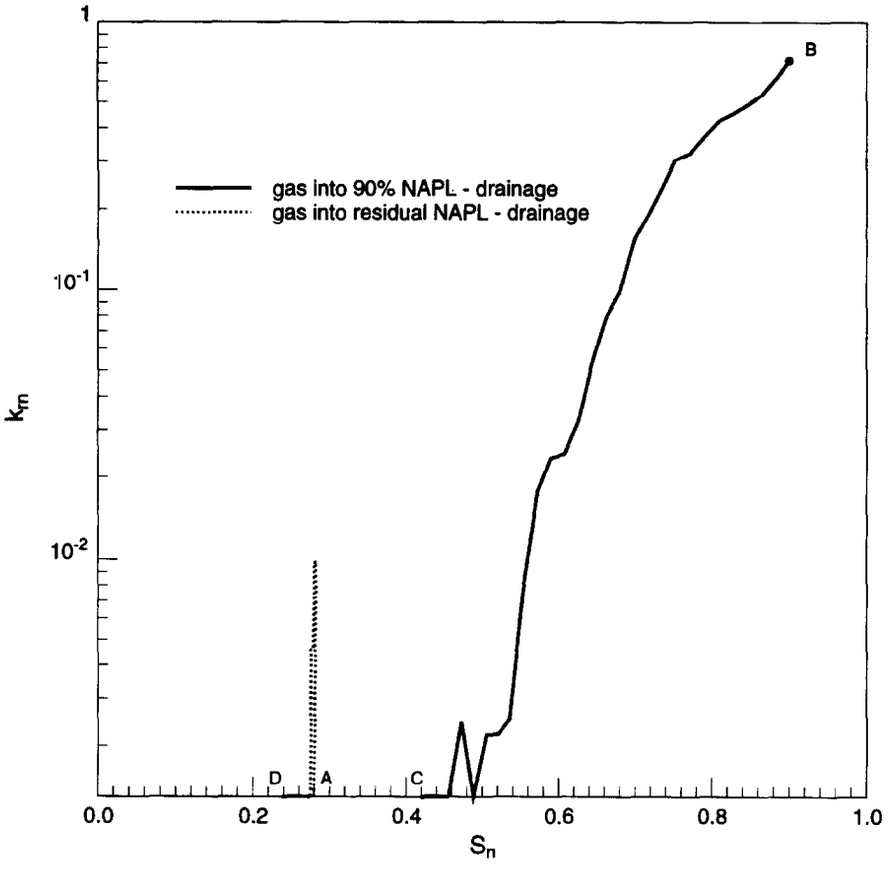

Fig. 23. NAPL relative permeability for $C_s^{eq} = -4$ mN/m displacements. The NAPL relative permeability for the gas into residual NAPL displacement is finite only when the NAPL becomes reconnected across the network. For gas invasion into 90% NAPL, the relative permeability falls to zero very rapidly, with increases in k_{rn} when NAPL reconnects.

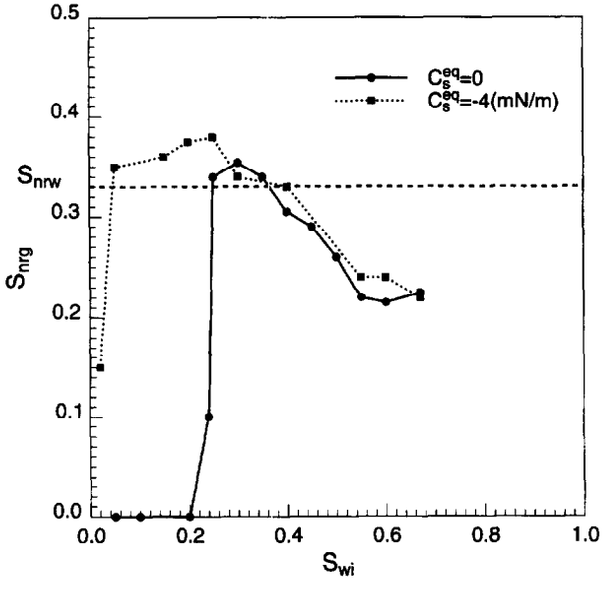

Fig. 24. Residual NAPL saturation after gas invasion as a function of the water saturation at the beginning of the gasflood. Note that for a certain range of water saturations the ultimate recovery can be worse than if only water displaced the NAPL to residual NAPL.

in the formation of a NAPL bank ahead of the gas front. Thus, gas contacts a high NAPL saturation (with a correspondingly large P_{cnw}), while mobilized NAPL accumulates ahead of the gas. This is how efficient displacements are achieved. The network model cannot predict directly whether or not a NAPL bank is formed.

How could the network model be used to predict relative permeabilities and capillary pressures for a given displacement? We may imagine that the network model represents a tiny section of a soil or rock, which during a displacement, always has approximately constant saturation which varies slowly. A route in capillary pressure space can be guessed and the corresponding relative permeabilities can then be computed. The relative permeabilities could then be used in a numerical material balance solution for the flow with the (known) macroscopic boundary conditions. This specifies a new sequence of capillary pressures which are used to compute a new set of relative permeabilities. A self-consistent prediction is made when the relative permeabilities calculated are consistent with the path in capillary pressure space.

8 CONCLUSIONS

NAPL layers between water and gas in the pore space

can exist in systems with a negative initial spreading coefficient. We have given an approximate expression for when such layers are stable. These layers allow NAPL to remain connected and to flow at very low saturation.

Three phase flow allows a series of six double displacement mechanisms where one phase displaces another that displaces a third. Double drainage and double imbibition are mechanisms that can mobilize previously trapped NAPL.

The conductance of NAPL layers in the pore space is sensitive to the boundary conditions at the NAPL/water and NAPL/gas interfaces.

Network modeling allows us to predict from physical principles the NAPL recovery, relative permeabilities and capillary pressures for a variety of different displacements.

Three phase relative permeabilities and capillary pressures are strong functions of saturation history and fluid properties and cannot be described adequately by any of the available empirical models. For a system with zero spreading coefficient, we found that both the gas and NAPL relative permeabilities displayed hysteresis, while for a negative spreading coefficient, all three relative permeabilities showed hysteresis.

ACKNOWLEDGMENTS

We would like to thank Pål-Eric Øren and Dengen Zhou for many helpful comments. Financial support of this work was provided by Grant DACA39-95-K-0075 from the Department of Defense, Grant DE-F21-89MC26253 from the Department of Energy and the Stanford University Petroleum Research Institute Gas Injection Affiliates Program.

REFERENCES

1. Abriola, L. M., *Multiphase Migration of Organic Compounds in a Porous Medium: A Mathematical Model*, first edition. Springer-Verlag, Berlin (1984).
2. Adamson, A. W., *Physical Chemistry of Surfaces*, fifth edition. John Wiley & Sons, New York (1990).
3. Baker, L. E., Three-phase relative permeability correlations. Paper SPE 17369, *Proceedings of the 1988 Sixth SPE/DOE Symposium on Enhanced Oil Recovery*, Tulsa, OK, April.
4. Batchelor, G. K., *An Introduction to Fluid Dynamics*, first edition. Cambridge University Press, Cambridge (1991).
5. Blunt, M., King, M. J. & Scher, H., Simulation and theory of two-phase flow in porous media. *Physical Rev. A*, **46,** (1992) 7680–99.
6. Blunt, M. J., Zhou, D. & Fenwick, D. H., Three phase flow and gravity drainage in porous media. *Transport in Porous Media*, **20** (1995) 77–103.
7. Bryant, S. & Blunt, M. J., Prediction of relative permeability in simple porous media. *Physical Rev. A*, **46** (1992) 2004–2011.
8. Chatzis, I., Kantzas, A. & Dullien, F. A. L., On the investigation of gravity-assisted inert gas injection using micromodels, long Berea sandstone cores, and computer-assisted tomography. Paper SPE 18284, *Proceedings of the 1988 63rd Annual Technical Conference and Exhibition of the SPE*, Houston, TX, October.
9. Delshad, M. & Pope, G. A., Comparison of the three-phase oil relative permeability models. *Transport in Porous Media*, **4** (1989) 59–83.
10. Diaz, C. E., Chatzis, I. & Dullien, F. A. L., Simulation of capillary pressure curves using bond correlated site percolation on a simple cubic network. *Transport in Porous Media*, **2** (3) (1987) 215–40.
11. Dong, M., Dullien, F. A. L. & Chatzis, I., Imbibition of oil in film form over water present in edges of capillaries with an angular cross-section. *J. Colloid & Interface Sci.*, **172** (1995) 278–88.
12. Dullien, F. A. L., *Porous Media: Fluid Transport and Pore Structure*, second edition. Academic Press, San Diego (1992).
13. Dullien, F. A. L., Zarcone, C., MacDonald, I. F., Collins, A. & Bochard, R. D. E., The effects of surface roughness on the capillary pressure curves and the heights of capillary rise in glass bead packs. *J. Colloid & Interface Sci.*, **127** (1989) 362–72.
14. Dumoré, J. M. & Schols, R. S., Drainage capillary pressure functions and the influence of connate water. *Soc. Petrol. Engineers J.*, **14** (1974) 437–44.
15. Fayers, F. J., Extension of Stone's Method 1 and conditions for real characteristics in three-phase flow. *SPE Reservoir Engng*, **4** (1989) 437–45.
16. Fenwick, D. H. & Blunt, M. J., Pore level modelling of three phase flow in porous media. *Proceedings of the 1995 8th European Symposium on Improved Oil Recovery*, Vienna, Austria, May.
17. Hayden, N. J. & Voice, T. C., Microscopic observation of a NAPL in a three-fluid-phase soil system. *J. Contaminant Hydrol.*, **12** (1993) 217–26.
18. Heiba, A. A., Davis, H. T. & Scriven, L. E., Statistical network theory of three-phase relative permeabilities. Paper SPE 12690, *Proceedings of the 1984 4th DOE/SPE Symposium on Enhanced Oil Recovery*, Tulsa, OK, April.
19. Heiba, A. A., Sahimi, M., Scriven, L. E. & Davis, H. T., Percolation theory of two-phase relative permeability. *SPE Reservoir Engng*, 7 (1992) 123–32.
20. Hirasaki, G. J., Structural interactions in the wetting and spreading of van der Waals fluids. *J. Adhesion Sci. Technol.*, **7** (3) (1993) 285–322.
21. Jerauld, G. R. & Salter, S. J., The effect of pore-structure on hysteresis in relative permeability and capillary pressure: pore-level modeling. *Transport in Porous Media*, **5** (1990) 103–51.
22. Joos, P. & Van Hunsel, J., Spreading of aqueous surfactant solutions on organic liquids. *J. Colloid Interface Sci.*, **106** (1985) 161–7.
23. Kalaydjian, F., Origin and quantification of coupling between relative permeabilities for two-phase flows in porous media. *Transport in Porous Media*, **5** (3) (1990) 215–29.
24. Kalaydjian, F. J.-M., Performance and analysis of three-phase capillary pressure curves for drainage and imbibition in porous media. Paper SPE 24878, *Proceedings of the 1992 67th Annual Technical Conference and Exhibition of the SPE*, Washington DC, October.
25. Kalaydjian, F. J.-M., Moulu, J-C., Vizika, O. & Munkerud, P. K., Three-phase flow in water-wet porous media: Determination of gas/oil relative permeabilities under various spreading conditions. Paper SPE 26671,

Proceedings of the 1993 68th Annual Technical Conference and Exhibition of the SPE, Houston, TX, October.
26. Kantzas, A., Chatzis, I. & Dullien, F. A. L., Enhanced oil recovery by inert gas injection. Paper SPE 17379, *Proceedings of the 1988 Sixth SPE/DOE Symposium on Enhanced Oil Recovery*, Tulsa, OK, April.
27. Lenormand, R. & Zarcone, C., Role of roughness and edges during imbibition in square capillaries, Paper SPE 13264, *Proceedings of the 1984 SPE Annual Technical Conference and Exhibition*, Houston, TX, September.
28. Lenormand, R., Touboul, E. & Zarcone, C., Numerical models and experiments on immiscible displacements in porous media. *J. Fluid Mechanics*, **189** (1988) 165.
29. Lenormand, R., Zarcone, C. & Sarr, A. Mechanisms of the displacement of one fluid by another in a network of capillary ducts. *J. Fluid Mechanics*, **135** (1983) 337–53.
30. Leverett, M. C., Flow of oil and water through unconsolidated sands. *Trans. AIME*, **132** (1938) 149.
31. Lowry, M. I. & Miller, C. T., Pore-scale modeling of nonwetting-phase residual in porous media. *Water Resour. Res.*, **31** (3) (1995) 455–73.
32. McDougall, S. R. & Sorbie, K. S., The impact of wettability on waterflooding: pore-scale simulation. *SPE Reservoir Engng*, **10** (1995) 208–13.
33. Naar, J. R., Wygal, R. & Henderson, R., Imbibition relative permeability in unconsolidated porous media. *Soc. Petrol. Engineeers J.*, **2** (1962) 13–7.
34. Nilsen, L. S., Øren, P. E., Bakke, S. & Henriquez, A., Prediction of relative permeability and capillary pressure from a pore model. Paper SPE 35531, *Proceedings of the 1996 European 3-D Reservoir Modelling Conference*, Stavanger, Norway, April.
35. Oak, M. J., Three-phase relative permeability of water-wet Berea. Paper SPE 20183, *Proceedings of the 1990 Seventh SPE/DOE Symposium on Enhanced Oil Recovery*, Tulsa, OK, April.
36. Oak, M. J., Baker, L. E. & Thomas, D. C., Three-phase relative permeability of Berea sandstone. *J. Petrol. Technol.*, **42** (1990) 1057–61.
37. Øren, P-E. & Pinczewski, W. V., The effect of wettability and spreading coefficients on the recovery of waterflood residual oil by miscible gasflooding. Paper SPE 24881, *Proceedings of the 1992 67th Annual Technical Conference and Exhibition of the SPE*, Washington DC, October.
38. Øren, P-E., Billiote, J. & Pinczewski, W. V., Mobilization of waterflow residual oil by gas injection for water-wet conditions. *SPE Formation Evaluation*, **7** (1992) 70–8.
39. Øren, P-E., Billiote, J. & Pinczewski, W. V., Pore-scale network modelling of waterflood residual oil recovery by immiscible gas flooding. Paper SPE 27814, *Proceedings of the 1994 Improved Oil Recovery Symposium*, Tulsa, OK, April.
40. Øren, P. E. & Pinczewski, W. V., The effect of film-flow on the mobilization of waterflood residual oil by gas flooding. *Proceedings of the 1991 6th European IOR Symposium*, Stavanger, Norway, May.
41. Parker, J. C., Lenhard, R. J. & Kuppusamy, T., A parametric model for constitutive properties governing multiphase flow in porous media. *Water Resour. Res.*, **23** (1987) 618–24.
42. Ransohoff, T. C. & Radke, C. J., Laminar flow of a wetting liquid along the corners of a predominantly gas-occupied noncircular pore. *J. Colloid Interface Sci.*, **121** (1988) 392–401.
43. Roof, J. G., Snap-off of oil droplets in water-wet pores. *Soc. Petrol. Engineers J.*, **10** (1970) 85–90.
44. Rowlinson, J. S. & Widom, B., *Molecular Theory of Capillarity*, first edition. Clarendon Press, Oxford (1989).
45. Skurdal, H., Hustad, O. St. & Holt, T., Oil recovery by gravity drainage during gas injection. *Proceedings of the 8th European Symposium on Improved Oil Recovery*, 1995, Vienna, Austria, May.
46. Soll, W. E. & Celia, M. A., A modified percolation approach to simulating three-fluid capillary pressure–saturation relationships. *Adv. Water Resour.*, **16** (2) (1993) 107–26.
47. Soll, W. E., Celia, M. A. & Wilson, J. L., Micromodel studies of three-fluid porous media systems: pore-scale processes relating to capillary pressure-saturation relationships. *Water Resour. Res.*, **29** (9) (1993) 2963–74.
48. Stone, H. L., Probability model for estimating three-phase relative permeability. *J. Petrol. Technol.*, **20** (1970) 214–8.
49. Stone, H. L., Estimation of three-phase relative permeability and residual data. *J. Canadian Petrol. Technol.*, **12** (1973) 53–61.
50. van Genuchten, M. T., A closed-form equation for predicting the hydraulic conductivity of unsaturated soils. *Soil Sci. Soc. Am. J.*, **44** (1980) 892–8.
51. Vizika, O., Effect of the spreading coefficient on the efficiency of oil recovery with gravity drainage. *Proceedings of the 1993 Symposium on Enhanced Oil Recovery*, presented before the Division of Petroleum Chemistry, Inc., Denver, CO.
52. Zhou, D. & Blunt, M. J., Effect of spreading coefficient on the distribution of light non-aqueous phase liquid in the subsurface. Journal of Contaminant Hydrology, **25** (1–2) (1997) 1–19.